DEVELOPMENT OF MULTICORE AND TAPERED CHALCOGENIDE FIBERS FOR SUPERCONTINUUM GENERATION

A THESIS SUBMITTED TO
THE GRADUATE SCHOOL OF ENGINEERING AND SCIENCE
OF BILKENT UNIVERSITY
IN PARTIAL FULFILLMENT OF THE REQUIREMENTS FOR
THE DEGREE OF
MASTER OF SCIENCE
IN
MATERIALS SCIENCE AND NANOTECHNOLOGY

By
Abba Usman Saleh
December 2016

DEVELOPMENT OF MULTICORE AND TAPERED CHALCOGENIDE FIBERS FOR SUPERCONTINUUM GENERATION
By Abba Usman Saleh
December 2016

We certify that we have read this thesis and that in our opinion it is fully adequate, in scope and in quality, as a thesis for the degree of Master of Science.

Bülend Ortaç(Advisor)

Mehmet Bayindir(Co-Advisor)

Halime Gül Yağlıoğlu

Aykutlu Dana

Approved for the Graduate School of Engineering and Science:

Ezhan Karaşan
Director of the Graduate School

ABSTRACT

DEVELOPMENT OF MULTICORE AND TAPERED CHALCOGENIDE FIBERS FOR SUPERCONTINUUM GENERATION

Abba Usman Saleh
M.S. in Materials Science and Nanotechnology
Advisor: Bülend Ortaç
December 2016

The dramatic spectral broadening of an electromagnetic radiation as it propagates through a nonlinear medium is called Supercontinuum generation. Supercontinuum generation is indeed regarded as one of the prominent phenomenon in nonlinear optics and photonics with burgeoning applications in various fields such as spectroscopy, early cancer diagnostics, gas sensing, food quality control, fluorescence microscopy e.t.c.

Supercontinuum generation in optical fibers is however associated with three fundamental challenges: minimization of input power threshold, maximization of output power as well as output spectrum of a supercontinuum. Two unique fabrication approaches namely "Direct tapering" and "Multicore fibers" were proposed to address the aforementioned challenges.

Chalcogenide nanowires were fabricated via direct tapering of chalcogenide glasses, and spectral broadening with extremely low peak power of $\sim$ 2 W was demonstrated. Multicore array of chalcogenide step index fibers were also fabricated using a new method. The fabricated step index fiber has a diameter $\sim$ 1.35 μm which was engineered to have a zero dispersion wavelength (ZDW) around 1100 nm with a pump of center wavelength at 1550 nm .Using split step Fourier method, it was shown that the fiber possesses a great potential for severe spectral broadening. Supercontinuum generation with the as drawn fiber, encountered challenges as well as proposed solutions were demonstrated and discussed.

Keywords: supercontinuum generation, zero dispersion wavelength (ZDW), chalcogenide, step index fiber, tapering.

ÖZET

SÜPERKESİNTİSİZ TAYF ÜRETİMİ İÇİN ÇOKLU ÇEKİRDEKLİ VE İNCELTİLMİŞ KALKOJEN FİBERLERİN GELİŞTİRİLMESİ

Abba Usman Saleh
Malzeme Bilimi ve Nanoteknoloji, Yüksek Lisans
Tez Danışmanı: Bülend Ortaç
Aralık 2016

Elektromanyetik radyasyonun, doğrusal olmayan bir ortamdan geçerken tayfının olağanüstü bir genişlikte açılmasına süperkesintisiz tayf üretimi denir. Süperkesintisiz tayf üretimi spektroskopi, erken kanser teşhisi, gaz tespiti, gıda kalite kontrolü, floresan mikroskopisi gibi farklı alanlarda çok sayıda uygulama olanağı sağlayan fotonik ve doğrusal olmayan optik bilimlerinde en öne çıkan olgulardan biri olarak kabul edilmektedir.

Optik fiberlerde süperkesintisiz tayf üretimi 3 temel sorun ile karşı karşıyadır: Tayf genişliğinin artırılmasının yanında giriş güç eşiğinin azaltılması ve çıkış günün artırılmasıdır. Söz konusu engellerin aşılması konusunda, iki yeni yaklaşım olarak "Direk inceltilmiş fiber"ve "Mikroyapılı fiber"üretimi önerilmiştir.

Kalkojen camların direk çekilmesiyle kalkojen nanoteller üretilmiş ve 2W gibi oldukça küçük optik güçlerde tayf genişlemesi gözlemlenmiştir. Yeni bir yöntemin kullanılmasıyla, ayrıca çok çekirdekli adım indeksli kalkojen fiberler üretilmiştir. Sıfır yayılım dalgaboyu (ZDW), pompalama dalga boyu olan 1550nm'de olacak şekilde tasarlanan adım indeksli fiberlerin çapları $1.3\mu m$'dur. Ayrık adımlı Fourier sayısal yöntemi kullanılarak, üretilen fiberlerin oldukça geniş tayf yaratmada büyük potansiyelleri olduğu gösterilmiştir. Çekilen fiberlerde süperkesintisiz tayf üretimi gösterilmiş ve bu sırada yaşanan zorluklar, aynı zamanda çözüm önerileri tartışılmış ve uygulamalı gösterilmiştir.

Anahtar sözcükler: Süperkesintisiz tayf üretimi, ZDW, kalkojen camlar, adım indeksli fiber, fiber inceltilmesi.

Acknowledgement

First and foremost, I would like to express my sincere gratitude to my parents for their support, prayers and for always being there for me. Thank you mum for always lending an ear to understand my problems, offering advices and solidarity to ensure my comfort and success. "Mama in ba ke ba sai rijiya!". Daddy thank you very much for believing in me and doing everything possible at any cost to see that we got a quality education. I would also like to seize this opportunity to extend my profound appreciation to Agata Szczodra (Pato!) for her love, care, understanding and support, and for also boosting my confidence whenever I am in a misfortune condition. My sincere appreciation to all my friends and family, thank you very much indeed!.

I would also like to express my appreciation to my advisors Prof. Dr. Mehmet Bayindir and Asst. Prof. Dr. Bulend Ortac for providing me a great research enviroment and guidance, and whose patience and understanding made my thesis possible.

My wholehearted gratitude goes to my mentor Dr. Ozan Aktas for his guidance and support, and from whom I have learned a lot during the course of my masters research.

Special thanks to Elif Uzcengiz and Umar Musa Gishiwa for helping me with certain devices. I would also like to extend my appreciation to all Bayindir group members and my office mates for providing a comfortable studying atmosphere.

Finally, I would like to acknowledge the financial support from Bilkent UNAM, ERC and TUBITAK.

"In memory of my dearest friend, Haruna Dayyabu (1991 - 2011)"

Contents

List of Figures

Chapter 1

Introduction

A physical phenomenon leading to a dramatic spectral broadening of laser pulses propagating through a nonlinear medium is referred to as Supercontinuum generation (SCG). It was first demonstrated in bulk glass by Alfano and Shapiro in early 1970s [1] (for an overview of early experiments on supercontinuum generation one can refer to [2]), and has since become the subject of various investigations in broad range of nonlinear media, including solids, organic and inorganic liquids, gases, and various types of waveguide. In a decade, the field of nonlinear optics went from inception to powerful demonstrations with burgeoning applications. SCG posses wide range of applications in such diverse fields as pulse compression, spectroscopy, early cancer diagnostics [3], gas sensing [4, 5], food quality control [6], fluorescence microscopy [7] and the design of tunable ultrafast femtosecond laser sources.These developments were due, in large part, to the emergence of highly efficient nonlinear systems and high intensity lasers. Starting with the laser side, several systems have been developed to provide high intensities required to drive the nonlinear processes underlying supercontinuum generation including Q-switched lasers [8], gain-switched lasers [9], and mode-locked lasers [10]. Mode-locked lasers in particular have become popular pump sources for supercontinuum due to their high peak power outputs (KW - MW), small footprint, low energy consumption, and high coherence properties. Progress on building enhanced nonlinear media has been equally impressive [11–13]. While

the first nonlinear optics demonstrations relied mainly on non-inversion symmetric crystalline media with χ^2 nonlinearity, with the invention of low loss optical fibers in early 1970s, it then became possible for amorphous materials such as silica to display strong χ^3 optical nonlinearity, due to the provision of sufficient interaction lengths of orders of magnitude in optical fibers as opposed to conventional nonlinear crystals. Hence, relatively low χ^3 nonlinearity materials like silica, can still demonstrate Strong nonlinear effects due to this enhanced interaction length. Consequently, experimental demonstration of the usefulness of optical fibers for nonlinear optics became feasible soon after [14–16].

In this study we focus on developing new fabrication techniques to address the fundamental challenges associated with supercontinuum generation in optical fibers, which are; minimization of input power threshold for supercontinuum generation, maximization of output power as well as output spectrum of a supercontinuum. To address these primary challenges, two unique approaches were developed, namely; direct tapering of chalcogenide glasses, and multicore chalcogenide fibers.

One may wonder why chalcogenide glasses? perhaps, the answer to this question can be extremely broad. The promising properties of chalcogenide materials, such as large transparency window of ~ 25 μm (as compared to silica which shows strong vibrational absorption in the near/mid infrared region) and strong optical nonlinearities (about $\sim$ 2-3 orders of magnitude greater than that of silica) [17]. Also low melting temperature [18] as well as flexibility are among the facts that made chalcogenide the material of choice for our techniques. The organization of the thesis is as follows: Chapter 2 gives a theoretical background regarding nonlinear optics in general, as well as numerical modelling of the the supercontinuum phenomena. Chapter 3 talks about the new novel technique for direct tapering of chalcogenide materials, demonstration of spectral broadening with extremely low input powers using this novel technique. Chapter 4 discusses a newly developed technique for fabricating multicore fibers, followed by demonstration of SCG, some of the encountered challenges as well as proposed unique solutions. Lastly, a comprehensive conclusion is given in Chapter 5.

Chapter 2

Nonlinear optics theoretical background

Light matter interaction has been an attractive topic for decades. Today it is clearly understood that light enables matter to oscillate at atomic or molecular level, which in turn re-emits light. In optics, intensity independent and intensity dependent phenomena are referred to as linear and nonlinear respectively. Moreover, in linear fiber optics, the medium (i.e. fiber) properties do not depend on the propagating signal. However, when the material properties are modified by the propagating signal itself, then that is described as nonlinear optics.

Fundamentally, the anharmonic motion of bound electrons under the influence of an applied field can be regarded as the origin of nonlinearity. Consequently, due to this anharmonic motion, the total polarization P induced by electric dipoles is not linear but rather satisfies more general relation as [19]

$$P = \varepsilon_0 \chi^1 E + \varepsilon_0 \chi^2 E^2 + \varepsilon_0 \chi^3 E^3 + ... \tag{2.1}$$

where ε_0 is the permittivity of a vacuum and χ^k (k = 1, 2, . . .) is k^{th} order susceptibility. The dominant contribution to P is provided by the first order

susceptibility (also known as linear susceptibility). The second order susceptibility is responsible for second harmonic generation and sum-frequency generation. However, for a symmetric molecule like silica and other glasses, the second order susceptibility contribution is very small, hence negligible. Therefore optical fibers are not considered to exhibit second order susceptibility. Obviously, the third order susceptibility is responsible for nonlinear effects such as (Self Phase Modulation (SPM), Cross Phase Modulation (CPM), Four Wave Mixing (FWM), etc. which will be discussed later) in fibers [20].

Thus, the refractive index and absorption coefficient of the medium in the presence of nonlinearity becomes

$$n = n_0 + n_2|E|^2 \tag{2.2}$$

$$\alpha = \alpha_0 + \alpha_2|E|^2 \tag{2.3}$$

The total refractive index of the medium becomes both a function of frequency and intensity. The first and second term on the right hand side of equation (2.2) represents the linear refractive index due to the first order susceptibility and the nonlinear refractive index due to the third order susceptibility respectively. The term n_2 is referred to as nonlinearity coefficient (also known as Kerr Nonlinearity), and it is material dependent. Hence, the total absorption α also contains both linear and nonlinear absorption terms α_0 and α_2 respectively as shown in equation (2.3).

2.1 Nonlinear schrodinger equation

In order to make an analysis for the propagation of light inside an optical fiber in the presence of nonlinearity, one has to modify the Maxwell equation in order to include the nonlinear term in the polarization (which is related to the displacement) which will affect the wave equation. Generally, Maxwell equations can be expressed as

$$\nabla \times \vec{E} = -\frac{\partial \vec{B}}{\partial t} \tag{2.4}$$

$$\nabla \times \vec{H} = \vec{J} + \frac{\partial \vec{D}}{\partial t} \tag{2.5}$$

$$\nabla \cdot \vec{D} = \rho \tag{2.6}$$

$$\nabla \cdot \vec{B} = 0 \tag{2.7}$$

where $\vec{E}$ and $\vec{H}$ stands for electric and magnetic field vectors respectively, $\vec{D}$ and $\vec{B}$ are electric and magnetic flux densities, while $\vec{J}$ and ρ are current and charge density respectively.

$\vec{D}$ and $\vec{B}$ which are related to the propagating field, can be expressed using the following equations [21]

$$\vec{D} = \varepsilon_0 \vec{E} + \vec{P} = \varepsilon_0 n^2 \vec{E} \tag{2.8}$$

$$\vec{B} = \mu_0 \vec{H} + \vec{M} \tag{2.9}$$

$$\vec{P} = \varepsilon_0 \chi^1 \vec{E} + \varepsilon_0 \chi^3 \vec{E^3} = \vec{P_L} + \vec{P_{NL}} \tag{2.10}$$

where ε_0 and μ_0 are dielectric permittivity and permeability of a vacuum (or free space) respectively, $\vec{M}$ stands for magnetization (i.e. magnetic polarization vector) and $\vec{P}$ is the induced electric polarization vector. Since optical fibers are nonmagnetic, then $\vec{M}$ becomes 0.

Note: In an optical fiber, it is assumed that there is no conduction current flowing. Therefore, $\vec{J}$ and ρ are taken to be 0. Hence, the Maxwell equation now becomes:

$$\nabla \times \vec{E} = -\frac{\partial \vec{B}}{\partial t} \tag{2.11}$$

$$\nabla \times \vec{H} = \frac{\partial \vec{D}}{\partial t} \tag{2.12}$$

$$\nabla \cdot \vec{D} = 0 \tag{2.13}$$

$$\nabla \cdot \vec{B} = 0 \tag{2.14}$$

Equation (2.2) can be rewritten as

$$n = n_0 + \delta n_{NL}. \tag{2.15}$$

where δn_{NL} represents change in refractive index due to nonlinearity, and by substituting for n in (2.8), D becomes

$$D = \varepsilon_0(n_0^2 + 2n_0\delta n_{NL})E = \varepsilon(\omega)E + P_{NL}. \tag{2.16}$$

$\varepsilon(\omega) = \varepsilon_0 n_0^2$, $P_{NL} = 2\varepsilon_0 n_0 \delta n_{NL}\vec{E}$, and $\delta n_{NL} = n_2|a|^2$, where $|a|^2$ stands for intensity.

Remember, we assumed a source free and nonmagnetic medium, we also assumed that the medium is uniform (i.e homogeneous) and isotropic. Therefore, since the material property in an isotropic medium is same everywhere within the medium, then we can solve for the fields in scalar form.

At this point, we can deduce a wave equation for an electromagnetic field propagating in an isotropic medium based on the aforementioned approximations, which takes the form

$$\nabla^2 E - \mu_0\varepsilon(\omega)\frac{\partial^2 E}{\partial t^2} = \mu_0\frac{\partial^2}{\partial t^2}P_{NL}. \tag{2.17}$$

In order to solve this equation, lets assume a time dependent formulation based on an envelop function separated from the carriers for both nonlinear polarization and the fields [22].

$$E = \frac{1}{2}[a(z,t)e^{i(\omega_0 t - \beta_0 z)} + c.c.] \tag{2.18}$$

$$P_{NL} = \frac{1}{2}[\tilde{P}_{NL}(z,t)e^{i\omega_0 t} + c.c.] \tag{2.19}$$

$$A(z,\omega) = \int a(z,t)e^{-i\omega t}dt \tag{2.20}$$

ω_0 and β_0 corresponds to center frequency and propagation constant respectively, z is the propagation direction and $\tilde{\omega} = \omega - \omega_0$. By substituting for (2.18), (2.19) and (2.20) in (2.17) and multiplying the left side of the equation by $\frac{1}{2}\int \frac{d\tilde{\omega}}{2\pi}e^{i\tilde{\omega}t}$, we obtain

$$\begin{aligned}\frac{1}{2}\int \frac{d\tilde{\omega}}{2\pi}e^{i\tilde{\omega}t}[(\beta(\omega)^2 - \beta_0^2)A - 2i\beta_0\frac{\partial A}{\partial z} + \frac{\partial^2 A}{\partial z^2}]e^{i(\omega_0 t - \beta_0 z)} \\ = \frac{\mu_0}{2}[-\omega_0^2\tilde{P}_{NL} + 2i\omega_0\frac{\partial \tilde{P}_{NL}}{\partial t} + \frac{\partial^2 P_{NL}}{\partial t^2}]e^{i\omega t}\end{aligned} \tag{2.21}$$

$\beta(\omega) = \omega^2\mu_0\varepsilon(\omega)$, and now using slowly varying envelop approximation in both space and time

$$|\frac{\partial^2 a}{\partial t^2}| \ll |\omega_0\frac{\partial a}{\partial t}| \ll \omega_0^2|a| \tag{2.22}$$

$$|\frac{\partial^2 a}{\partial z^2}| \ll |\beta_0\frac{\partial a}{\partial z}| \ll \beta_0^2|a| \tag{2.23}$$

The second order term in left hand side of (2.21) and both first order and second order terms in right hand side of (2.21) can be neglected, then we have

$$\frac{1}{2}\int \frac{d\tilde{\omega}}{2\pi}e^{i\tilde{\omega}t}[(\beta(\omega)^2 - \beta_0^2)A - 2i\beta_0\frac{\partial A}{\partial z}] = -\frac{\mu_0}{2}\omega_0^2\tilde{P}_{NL}e^{i\beta_0 z} \tag{2.24}$$

The quantity $\beta(\omega)$ is very close to β_0 since we are talking about narrow band frequencies, therefore one can make an approximation

$$\beta(\omega)^2 - \beta_0^2 = (\beta(\omega) - \beta_0)(\beta(\omega) + \beta_0) \approx 2\beta_0(\beta(\omega) - \beta_0) \tag{2.25}$$

then equation (2.24) becomes

$$\frac{1}{2}\int \frac{d\tilde{\omega}}{2\pi} e^{i\tilde{\omega}t}[2\beta_0(\beta(\omega)-\beta_0)A - 2i\beta_0\frac{\partial A}{\partial z}] = -\frac{\mu_0}{2}\omega_0^2\tilde{P}_{NL}e^{i\beta_0 z} \tag{2.26}$$

Since we are dealing with a band of frequencies $\beta(\omega) \neq \beta_0$ everywhere but rather varies with respect to β_0, therefore one can have a Taylors expansion series for $\beta(\omega)$ around β_0.

$$\beta(\omega) = \beta_0 + (\omega-\omega_0)\frac{\partial\beta}{\partial\omega}|_{(\omega=\omega_0)} + \frac{(\omega-\omega_0)^2}{2}\frac{\partial^2\beta}{\partial\omega^2}|_{(\omega=\omega_0)} + ... - i\frac{\alpha}{2} \tag{2.27}$$

$\beta_n \cong \frac{\partial^n\beta}{\partial\omega^n}|_{(\omega=\omega_0)}$, for n = 1,2,3,.....

We added a loss term α because the pulse experience some losses as it propagates along the fiber. Also as mentioned previously $P_{NL} = 2\varepsilon_0 n_0 n_2|a|^2E = 2\varepsilon_0 n_0 n_2|a|^2 a e^{i(\omega_0 t-\beta_0 z)}$, by substituting for P_{NL} and multiplying both sides of the equation by $\frac{i}{2\beta_0}$ in (2.26), we obtain

$$\int \frac{d\tilde{\omega}}{2\pi} e^{i\tilde{\omega}t}[\frac{\partial A}{\partial z} + i(\beta_1\tilde{\omega} + \frac{\beta_2}{2}\tilde{\omega}^2 + ...)A + \frac{\alpha}{2}A] = -i\frac{\omega_0^2}{\beta_0}\mu_0\varepsilon_0 n_0 n_2|a|^2 a \tag{2.28}$$

$$\frac{1}{c} = \frac{\omega_0}{\beta_0}\mu_0\varepsilon_0 n_0 \tag{2.29}$$

by substituting for (2.29) in (2.28) and solving the equation, we have

$$\frac{\partial a}{\partial z} + \beta_1\frac{\partial a}{\partial t} - i\frac{\beta_2}{2}\frac{\partial^2 a}{\partial t^2} + \frac{\alpha}{2}a + i\frac{\omega_0}{c}n_2|a|^2 a = 0 \tag{2.30}$$

So far we have been dealing with the pulse evolution along propagation direction z, now lets include a transverse function $U(x,y)$ which gives information about the modal distribution of the field. The field now takes the form

$a(z,t)e^{i(\omega_0 t-\beta_0 z)}U(x,y)$. An important approximation worth mentioning here, is that the mode shape is independent of frequency. By including the tranverse function U in equation (2.30), multiplying by U^* and integrating over the transverse coordinate (dx, dy), we obtain

$$\int\int dxdy[\frac{\partial a}{\partial z}+\beta_1\frac{\partial a}{\partial t}-i\frac{\beta_2}{2}\frac{\partial^2 a}{\partial t^2}+\frac{\alpha}{2}a]+i\frac{\omega_0}{c}n_2|a|^2a\frac{\int\int|U|^4dxdy}{\int\int|U|^2dxdy}=0 \quad (2.31)$$

Lets write our equation interms of normalized power rather than intensity, such that $|a_p|^2=\int\int|a|^2dxdy$. After substitution, (2.31) yields

$$\frac{\partial a_p}{\partial z}+\beta_1\frac{\partial a_p}{\partial t}-i\frac{\beta_2}{2}\frac{\partial^2 a_p}{\partial t^2}+\frac{\alpha}{2}a_p+i\gamma|a_p|^2a_p=0 \quad (2.32)$$

$$\gamma=\frac{n_2\omega_0}{cA_{eff}} \qquad A_{eff}=\frac{(\int\int|U|^2dxdy)^2}{\int\int|U|^4dxdy} \quad (2.33)$$

Equation (2.32) is referred to as Nonlinear Schrodinger Equation, where $\frac{\partial a_p}{\partial z}$ gives information about the pulse envelop evolution along the fiber, γ is the nonlinearity parameter, A_{eff} is the effective area within which the light is confined inside the fiber, c is speed of light, β_1 is the group delay, β_2 is the group velocity dispersion and α represents losses.

2.2 Linear pulse propagation

When the intensity of a propagating signal in an optical fiber is insufficient to trigger a nonlinear phenomenon, this type of propagation is term Linear Propagation. Such type of propagation is associated with attenuation and Dispersion phenomenon, which will be explained in details later in this chapter.

2.2.1 Dispersion

Dispersion is an effect originated from the frequency dependence of the refractive index of a medium, and tend to disperse a pulse propagating inside the medium. There are several types of dispersion namely Modal, Inter-modal and Chromatic Dispersion. However, in this thesis our focus will be mainly on Chromatic Dispersion. In this regard, dispersion is classified into Material and Waveguide dispersion.

Material dispersion is associated with the frequency dependence of the refractive index of the bulk material, while the effective index change due to modal confinement is referred to as waveguide dispersion [23] which may vary depending on the size and geometry of the waveguide.

Far from the medium resonances, the refractive index variation can be obtained using Sellmeier equation [20]

$$n^2 = 1 + \sum_{i=1}^{m} \frac{B_i \omega_i^2}{\omega_i^2 - \omega^2} \tag{2.34}$$

where ω_i and B_i are the resonance frequency and strength of the i^{th} resonance respectively.

Using Taylor expansion series around the center frequency ω_0 as shown above in equation (2.27), we can obtain the propagation constant β

$\beta_n \cong \frac{\partial^n \beta}{\partial \omega^n}|_{(w=w_0)}$ for n= 1,2,3,.....

β_1 is related to the group velocity as,

$$\beta_1 = \frac{1}{v_g} = \frac{n_g}{c} = \frac{1}{c}(n + \omega \frac{\partial n}{\partial \omega}) \tag{2.35}$$

where β_2 stands for Group Velocity Dispersion (GVD), which shows frequency dependence of the group velocity.

$$\beta_2 = \frac{\partial}{\partial\omega}[\frac{1}{v_g}] = \frac{1}{c}(2\frac{\partial n}{\partial\omega} + \omega\frac{\partial^2 n}{\partial\omega^2}) \tag{2.36}$$

Higher order β parameters can also be observed, but their contribution is quite negligible unless in the presence of extremely short pulses or while pumping at $\beta_2 = 0$ (i.e. the zero dispersion wavelength (ZDW)). However, the term β_2 happens to be very crucial because its sign determines the dispersion regime. Where $\beta_2 > 0$ and $\beta_2 < 0$ corresponds to Normal and Anomalous dispersion regimes respectively. In the anomalous dispersion regime a negative frequency chirping is observed while in the normal dispersion regime is vice verse. Either way, the pulse experiences broadening in the temporal domain.

It is important to know that, there is a certain characteristic length at which dispersion/nonlinear phenomenon is manifested.

$$L_D = \frac{T_0^2}{|\beta_2|} \qquad\qquad L_{NL} = \frac{1}{\gamma P_0} \tag{2.37}$$

L_D and L_{NL} are the dispersion and nonlinear length respectively, where T_0 is the pulse width, β_2 is the group velocity dispersion, γ is nonlinear parameter and P_0 is the peak power.

Now assuming loss $\alpha = 0$ in the fiber and L is the fiber length, then we have 3 possibilities:

$L \ll L_D, \qquad L \ll L_{NL}$ Fiber is just a medium to transport light.

$L \gg L_D, \qquad L \ll L_{NL}$ Dispersion becomes dominant (pulse broadening).

$L \ll L_D, \qquad L \gg L_{NL}$ Self Phase Modulation (and other nonlinearities).

2.2.2 Group velocity dispersion (β_2)

The preceding subsection showed how the combined effect of Nonlinearity and that of Group Velocity Dispersion(GVD) on an optical signal propagating inside a fiber, can be studied via solving an envelope equation of the propagating signal. We have also seen that, the sign of β_2 determines the two dispersion regimes, namely normal and anomalous dispersion regime (for positive and negative signs respectively). Different frequency chirping behavior as well as pulse broadening and compression occurs, depending on the input pulse parameters as well as the dispersion regime of the optical waveguide.

Now assuming a pulse width greater than 5 ps, then we can use the Nonlinear Schrodinger Equation in the form

$$\frac{\partial a_p}{\partial z} + \frac{\alpha}{2}a_p - i\frac{\beta_2}{2}\frac{\partial^2 a_p}{\partial T^2} = i\gamma|a_p|^2 a_p \tag{2.38}$$

where a_p is the amplitude of the slowly varying envelope, $T = t - \frac{z}{v_g}$.

Let us introduce a normalized amplitude 'U' as well as a normalized time scale 'τ' to the input pulse width, where $a_p(z,\tau) = \sqrt{P_0}\exp -\frac{\alpha z}{2}U(z,\tau)$ and $\tau = \frac{T}{T_0}$. Now by substituting these parameters into (2.38), and remember the effects of GVD on an optical signal propagating inside a linear medium [24–28] can be studied by setting α and γ (i.e. the loss and nonlinearity terms) to 0, then we have

$$\frac{\partial U}{\partial z} = -i\frac{\beta_2}{2}\frac{\partial^2 U}{\partial T^2} \tag{2.39}$$

by taking the Fourier transform of the normalized amplitude 'U' and solving (2.39) we obtain

$$\tilde{U}(z,\omega) = \tilde{U}(0,\omega)e^{i\frac{\beta_2}{2}\omega^2 z} \tag{2.40}$$

This is the solution in the Fourier domain for the Nonlinear Schrodinger Equation when only the dispersion effect is present. The first term on the right is the

initial amplitude spectrum of the pulse, while the second term with the exponential is responsible for phase change, hence, frequency chirping. Note that, during GVD the amplitude spectrum of the pulse remains unchanged, only different frequency components undergo a phase change. Furthermore, the spectrum in the presence of GVD does not get modified, however, since different frequency components will undergo a phase change, the function of the pulse gets modified, as a result, the amplitude function or the pulse shape gets modified. One can take an Inverse Fourier transform of (2.40) in order to find out what the pulse shape would be in time domain. The inverse Fourier transform is given as

$$U(z,T) = \frac{1}{2\pi}\int_{-\infty}^{+\infty} \tilde{U}(0,\omega) exp^{(i\frac{\beta_2}{2}\omega^2 z - i\omega T)} d\omega. \tag{2.41}$$

For instance, consider a Gaussian pulse where the incident field takes the form [28]

$$U(0,T) = exp[-\frac{T^2}{2T_0^2}] \tag{2.42}$$

for a Gaussian pulse $T_{FWHM} = 2(\ln 2)^{\frac{1}{2}} T_0 \approx 1.665 T_0$.

By substituting for the Gaussian pulse in (2.41) and solving the integral we obtain

$$U(z,T) = \frac{T_0}{(T_0^2 - i\beta_2 z)^{\frac{1}{2}}} exp[-\frac{T^2}{2(T_0^2 - i\beta_2 z)}] \tag{2.43}$$

$$T_1(z) = T_0[1 + (\frac{z}{L_D})^2]^{\frac{1}{2}} \tag{2.44}$$

Equation (2.44) means at $z = L_D$ the pulse broadens by a factor of $\sqrt{2}$, at $L_D \gg z$ the pulse undergoes no broadening at all, while at $L_D \ll z$ a severe broadening of the pulse is observed in time domain. By comparing Eqs (2.42) to (2.43) it can be seen that although the incident pulse is unchirped, the transmitted pulse becomes chirped. And this can be clearly seen by writing $U(z,T)$ as

$$U(z,T) = |U(z,T)| exp[i\phi(z,T)] \tag{2.45}$$

where

$$\phi(z,T) = -\frac{sgn(\beta_2)(\frac{z}{L_D})}{1+(\frac{z}{L_D})^2}\frac{T^2}{2T_0^2} + \frac{1}{2}\tan^{-1}(sgn(\beta_2)\frac{z}{L_D}). \tag{2.46}$$

The phase varies quadratically across the pulse at any distance z. The frequency modulation or the frequency chirping $\delta\omega$ can be obtained by taking the derivative of the phase variation as a function of time as shown below

$$\delta\omega = -\frac{\partial\phi}{\partial T} = \frac{sgn(\beta_2)(\frac{z}{L_D})}{1+(\frac{z}{L_D})^2}\frac{T}{T_0^2} \tag{2.47}$$

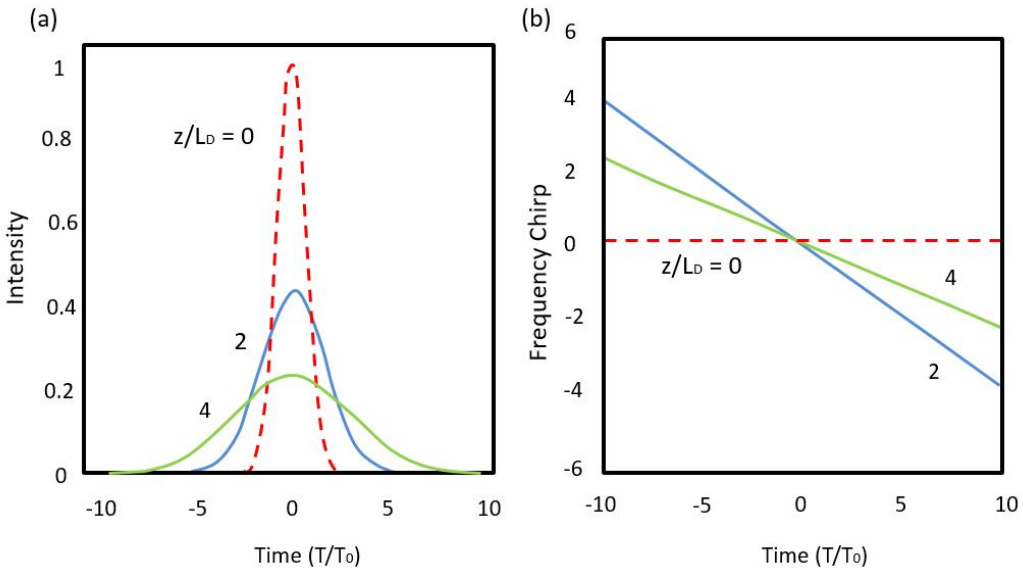

Figure 2.1: (a) and (b)shows normalized intensity broadening and frequency chirping as a function of time respectively for a Gaussian pulse at $z = 2L_D$ and $z = 4L_D$. Note dashed lines represents input profiles at z=0 [29]

As can be seen in Fig 2.1 (a), the incident pulse undergoes a temporal broadening as it propagates along the fiber. And (b) shows the frequency chirping where we have a positive or negative values for positive and negative frequency chirping.

As we have seen for an initially unchirped Gaussian pulse in (2.42), GVD induced broadening does not depend on the sign of β_2 . Thus, the pulse broadens

equally by the same magnitude in both normal and anomalous dispersion regimes of the fiber with a given dispersion length of L_D. However, this behavior changes when the incident pulse is initially chirped [27]. An initially chirped incident Gaussian pulse can be expressed by modifying equation (2.42) to include the chirping parameter 'C' as

$$U(0,T) = exp[-\frac{(1+iC)}{2}\frac{T^2}{2T_0^2}]. \tag{2.48}$$

Using the same analysis as in the case of an initially unchirped Gaussian pulse (as shown previously) for the initially chirped one, and replacing the initial amplitude of the former by the latter, one will see that the frequency increases linearly from the leading to the trailing edge (up-chirp) for $C > 0$. Meanwhile, the opposite occurs (down-chirp) for $C < 0$. It is common to refer to the chirp as being positive or negative, depending on whether C is positive or negative.

Moreover, similar scenario holds for other kind of pulses (such as hyperbolic secant pulses) for the initially chirped and unchirped conditions. Also the effects of higher order dispersion (such as third order dispersion and so on) should be considered and be included in the Nonlinear Schrodinger Equation, especially when pumping in/near the zero dispersion wavelength (i.e. where $\beta_2 \approx 0$) or when using an ultra short pulse (with width $T_0 < 1ps$).

2.3 Nonlinear pulse propagation

Nonlinear effects in optical fiber occur either due to the medium refractive index dependence on intensity (which is referred to as Kerr effect) or due to inelastic scattering phenomena [30]. The power dependence of the refractive index is responsible for Kerr effect. The Kerr effect manifest itself in three different nonlinear effects namely Cross Phase Modulation (CPM), Self Phase Modulation (SPM) and Four Wave Mixing (FWM) depending upon the power of the incident pulse. The inelastic scattering phenomena comes into play at high power

level, inducing stimulated effects such as Stimulated Raman Scattering (SRS) and Stimulated Brillouin Scattering (SBS). The main difference between Stimulated Raman Scattering (SRS) and Stimulated Brillouin Scattering (SBS) is that, the phonons (acoustic) generated in SBS are coherent, consequently leads to macroscopic acoustic wave in the fiber whereas the phonons (optical) in SRS are incoherent, hence, no macroscopic wave is generated [30].

2.3.1 Self Phase Modulation (SPM)

An astonishing manifestation of Kerr effect in nonlinear optical media occurs through self phase modulation (SPM), such a phenomenon leads to spectral broadening of optical signal [31–35]. In order to have a better insight of SPM, a clear understanding of nonlinear phase shift is absolutely crucial. Similar to equation (2.39), lets assume there is no loss in the medium (i.e. $\alpha = 0$) as well as GVD is 0 but nonlinearity exists in the fiber (i.e. $\gamma \neq 0$), then we have

$$\frac{\partial U}{\partial z} = \frac{ie^{-\alpha z}}{L_{NL}}|U|^2 U \tag{2.49}$$

where α is fiber loss and $L_{NL} = \frac{1}{\gamma P_0}$ which is the nonlinear length.

Equation (2.49) can be solved by using $U = Ve^{i\phi_{NL}}$ and equating the real and imaginary parts so that

$$\frac{\partial V}{\partial z} = 0 \qquad \frac{\partial \phi_{NL}}{\partial z} = \frac{e^{-\alpha z}}{L_{NL}}V^2. \tag{2.50}$$

As can be seen V remains constant across the fiber length, while the phase equation can be integrated analytically to get a general solution

$$U(L,T) = |U(0,T)|e^{i\phi_{NL}(L,T)} \tag{2.51}$$

then

$$\phi_{NL}(L,T) = |U(0,T)|^2 \frac{L_{eff}}{L_{NL}} \tag{2.52}$$

where U(0,T) is the initial amplitude at $z = 0$ and $L_{eff} = [\frac{(1-e^{-\alpha L})}{\alpha}]$ is the effective length of a fiber, which is smaller than the initial length L because of losses in the fiber. However, in a lossless medium ($i.e. \alpha = 0$), $L = L_{eff}$. It is apparent from (2.52) that SPM yields an intensity dependent phase shift. The maximum phase shift occurs at the center of the pulse at ($T = 0$) which corresponds to $U(0, 0) = 1$, where

$$\phi_{max} = \frac{L_{eff}}{L_{NL}} \tag{2.53}$$

The time dependence of ϕ_{NL} leads to spectral changes induced by SPM. Similar to (2.47), the temporally varying phase implies that the instantaneous optical frequency differs across the pulse from its central value ω_0. The difference $\delta\omega$ (frequency chirp) is given by

$$\delta\omega(T) = -\frac{\partial\phi_{NL}}{\partial T} = -\frac{L_{eff}}{L_{NL}}\frac{\partial|U(0,T)|^2}{\partial T} \tag{2.54}$$

The frequency chirp induced by SPM leads to generation of new frequency components as the pulse propagates along the fiber length which broadens the spectrum of the initially unchirped pulse.

It is also important to mention that the output spectrum depends on the input pulse shape as well as the initial chirping parameter of the pulse. For instance, a pulse with steep leading and trailing edge such as a Super Gaussian pulse, where the frequency range of the SPM induced chirp is larger compared to that of a normal unchirped Gaussian pulse. An initial frequency chirp can also lead to drastic changes in the SPM broadened pulse spectrum. Chirping plays a critical role depending on the sign of the chirping parameter C. For $C > 0$ spectral broadening increases and the oscillatory structure in the output spectrum becomes less pronounced. However, $C < 0$ leads to spectral narrowing through SPM because the two chirp contributions are of opposite signs.

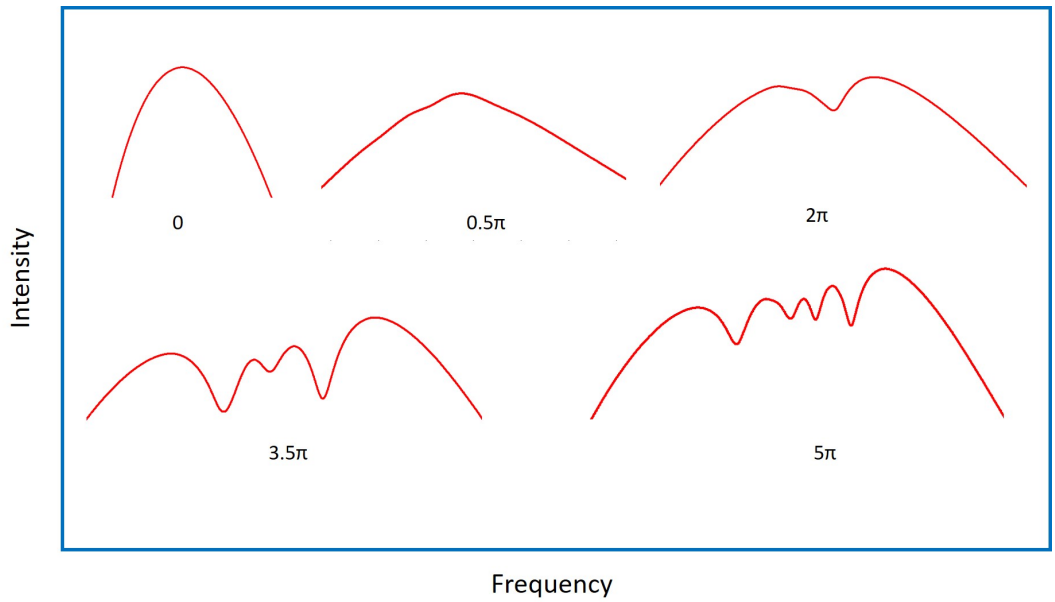

Figure 2.2: SPM-broadened spectra for an unchirped Gaussian pulse. Spectra are labelled by the maximum nonlinear phase shift ϕ_{max}.

So far in this section we have assumed relatively long pulses (T_0 <50 ps) propagating along the fiber, for which the dispersion length is much larger compared to the fiber (L) and nonlinear length (L_{NL}). As pulses become shorter, the dispersion length becomes comparable to the fiber length, then it becomes necessary to consider the combine effects of GVD and SPM [35]. An interplay between SPM and GVD in the anomalous dispersion regime of an optical fiber leads to a phenomenon where the pulse propagates as an optical soliton [36, 37] (which will be discussed later in this chapter). However, the combined effect of SPM and GVD in the normal dispersion regime leads to enhanced pulse broadening rate compare to that of GVD alone.

2.3.1.1 Soliton

Assuming we maintain a certain pulse width and power sufficient enough to trigger nonlinearity in an optical fiber, and pumping in the anomalous dispersion regime. An interplay between SPM induced frequency chirping (which is linear and positive) and that of GVD (which is negative) balanced each other, which

leads to pulse propagating extremely long distances without any distortion. This phenomenon is referred to as SOLITON [37].

Again lets consider the NLSE equation for a better understanding of the soliton dynamics, but now assuming dispersion contribution is present where as that of loss remains 0. By introducing some normalized parameters

$$\xi = \frac{z}{L_D}, \qquad \tau = \frac{T}{T_0}, \qquad N^2 = \frac{L_D}{L_{NL}} = \frac{\gamma P_0 T_0^2}{|\beta_2|} \tag{2.55}$$

then NLS takes the form:

$$\frac{\partial U}{\partial \xi} - isgn(\beta_2)\frac{1}{2}\frac{\partial^2 U}{\partial \tau^2} + iN^2|U|^2U = 0 \tag{2.56}$$

The term N is defined as Soliton number or Order of a soliton, which governs the relative importance of the GVD and SPM effects along fiber upon pulse propagation. SPM related effects dominate for $N >> 1$ while GVD dominates for $N << 1$, and for $N \approx 1$ both SPM and GVD have equal contribution to the propagating pulse.

Now lets define $U = \frac{u}{N}$, and assuming pumping in the anomalous regime i.e. $\beta_2 < 0$, then $sgn(\beta_2) = -1$ by substituting for these terms in equation (2.56) we have

$$\frac{\partial u}{\partial \xi} + i\frac{1}{2}\frac{\partial^2 u}{\partial \tau^2} + i|u|^2u = 0. \tag{2.57}$$

This needs to be solved using the inverse scattering method when $N > 1$ however, for our case where $N = 1$ this equation can be solved rather easily since we are looking for a phenomenon where the pulse shape remains intact (i.e. undistorted). One can solve this equation by assuming

$$u(\xi, \tau) = V(\tau)e^{i\phi(\xi,\tau)} \tag{2.58}$$

where V is a function of time but doesn't change with propagation length and ϕ is a phase constant which is both a function of time and space.

By substituting (2.58) into (2.57), separating real and imaginary parts, we will be left with two equations

$$\phi(\xi,\tau) = -K\xi + \delta\tau \qquad for \qquad \delta = 0 \qquad then \qquad \phi(\xi,\tau) = -K\xi \tag{2.59}$$

K stands for phsae constant and δ is the frequency shift. And the other equation (i.e. for V) can be obtained as

$$\frac{d^2V}{d\tau^2} = 2V(K - V^2) \tag{2.60}$$

the above equation can be solved by multiplying both sides by $2\frac{dV}{d\tau}$ and then integrate it as a function of τ we have

$$\int 2\frac{dV}{d\tau}\frac{d^2V}{d\tau^2}d\tau = \int 2V(K - V^2)2\frac{dV}{d\tau}d\tau \tag{2.61}$$

let

$$I = \int 2\frac{dV}{d\tau}\frac{d^2V}{d\tau^2}d\tau$$

using integration by part I can be solved as

$$I = 2(\frac{dV}{d\tau})^2 - I$$

then

$$I = (\frac{dV}{d\tau})^2$$

by substituting for I in (2.61) we have

$$(\frac{dV}{d\tau})^2 = \int 4V(K - V^2)dV$$
$$= 2KV^2 - V^4 + C$$

C is an integration constant, and can be obtained by applying boundary condition

$$V = 0, \quad \frac{dV}{d\tau} = 0, \quad \tau \to \infty$$

$$C = 0$$

Finally we obtain a solution to (2.61) as

$$(\frac{dV}{d\tau})^2 = V^2 - V^4, \qquad \frac{dV}{d\tau} = V\sqrt{1 - V^2}$$

after integration we have

$$V = sech(\tau) \tag{2.62}$$

We obtain a final solution for the NLS equation as

$$u(\xi, \tau) = sech(\tau)e^{-\frac{i\xi}{2}} \tag{2.63}$$

Remember we assumed $L_{NL} = L_D$ which corresponds to $N = 1$ and this is referred to as fundamental soliton, hence the above equation is an excellent manifestation of the pulse shape of a fundamental soliton. An important phenomenon where higher order solitons breaks into fundamental solitons generating dispersive waves, is termed Soliton fission [38].

2.3.2 Cross Phase Modulation (XPM)

So far we have considered just a single signal propagating inside the optical fiber, and we have seen that the refractive index depends on the intensity inside the

fiber. Assuming rather than a single signal, we have multiple signals propagating simultaneously inside the optical fiber. Two different phenomena occur namely, Cross phase modulation (XPM) and Four wave mixing (FWM). Both of these phenomena are related to the third order susceptibility term χ^3. In this subsection we will be discussing XPM whereas FWM will be discussed in the subsequent subsection. XPM is often accompanied by SPM, because both the signal intensity itself and that of the co propagating signals contributes to the nonlinear refractive index modulation. [39].

Assuming we have an electric field which has two frequency components:

$$E = E_1 e^{i\omega_1 t} + E_2 e^{i\omega_2 t} \tag{2.64}$$

by substituting for the electric field into the polarization expression the nonlinear polarization term (P_{NL}) becomes

$$P_{NL} = P_{NL}(\omega_1)e^{i\omega_1 t} + P_{NL}(\omega_2)e^{i\omega_2 t} + P_{NL}(2\omega_1 - \omega_2)e^{i(2\omega_1 - \omega_2)t} + ... \tag{2.65}$$

where

$$P_{NL}(\omega_1) = \chi^3\{|E_1|^2 + 2|E_2|^2\}E_1$$

$$P_{NL}(\omega_2) = \chi^3\{|E_2|^2 + 2|E_1|^2\}E_2$$

Because of these nonlinearities, the change in refractive index Δn_j at any frequency j takes the form

$$\Delta n_j \approx n_2\{|E_j|^2 + 2|E_{3-j}|^2\}. \tag{2.66}$$

The first term in above equation represents the contribution of SPM and second term that of XPM.The most important thing to note here is that the change in refractive index due XPM has an enhancement factor of 2 compared to that of SPM, which indicates that XPM is twice as effective as SPM for the same amount

of power. Remember in a case where we have a propagating signal, the change in phase is caused by the signal itself (i.e. via SPM). However, in the presence of a co-propagating signal, the change in phase is not only caused by the signal itself, but rather due to both the signal and the co-propagating signal. And this phenomenon is referred to as Cross Phase Modulation (XPM). The nonlinear phase change can be written as

$$\phi_{NL} = \frac{\omega_j}{c}\Delta n_j z, \qquad where \qquad j = 1, 2, ...$$

.

In the absence of XPM that is when SPM acts alone, the induced spectral broadening is symmetric in shape, however, when there is a group velocity mismatch between the signals, the combined effects of SPM and XPM results in an assymmetric spectral broadening.

Similarly, the field distribution in XPM can be written as

$$E_j = U_j(x, y)a_j(z)e^{-i\beta_{0j}z} \tag{2.67}$$

by following the same procedure as we did previously for a single propagating signal, the NLS takes the form

$$\frac{\partial a_j}{\partial z} + \beta_{1j}\frac{\partial a_j}{\partial t} - i\frac{\beta_{2j}}{2}\frac{\partial^2 a_j}{\partial t^2} + \frac{\alpha_j}{2}a_j = -i\frac{n_2\omega_j}{c}\{f_{jj}|a_j|^2 + 2f_{jk}|a_k|^2\}a_j \tag{2.68}$$

The term f_{jk} is referred to as the overlap integral, which is given by

$$f_{jk} = \frac{\int\int |U_j(x, y)|^2|U_k(x, y)|^2 dxdy}{\int\int |U_j(x, y)|^2 dxdy \int\int |U_k(x, y)|^2 dxdy} \tag{2.69}$$

for

$$j = k,$$

$$f_{jk} = \frac{1}{A_{eff}}$$

then the NLS equation finally becomes

$$\frac{\partial a_j}{\partial z} + \beta_{1j}\frac{\partial a_j}{\partial t} - i\frac{\beta_{2j}}{2}\frac{\partial^2 a_j}{\partial t^2} + \frac{\alpha_j}{2}a_j = -i\gamma\{|a_j|^2 + 2|a_k|^2\}a_j \tag{2.70}$$

Note: XPM is effective only when the interacting signals superimpose in time.

2.3.3 Four Wave Mixing (FWM)

This phenomena is analogous to inter channel mixing or inter modulation products in electronic systems. We know that when an amplifier goes into saturation, if you put two frequencies inside the amplifier a third frequency is generated. Exactly same phenomena occurs in optical fibers which originates from the third order susceptibility χ^3. Now consider the nonlinear polarization term P_{NL} for three simultaneously propagating signals of different center frequencies as

$$P_{NL} = \varepsilon_0 \chi^3 \vdots E_1 E_2 E_3 \tag{2.71}$$

The three frequencies ω_1, ω_2 and ω_3 co-propagating inside the fiber will generate a fourth frequency ω_4

$$\omega_4 = \omega_1 \pm \omega_2 \pm \omega_3$$

$$k_4 = k_1 \pm k_2 \pm k_3$$

where k and ω stands for phase constant and frequency respectively, several frequency and phase combinations are possible. However, effective combination during FWM process depends on the phase mismatch between electric field and

polarization components. Significant FWM occurs only if the phase mismatch nearly vanishes [40]. In quantum-mechanical context, FWM occurs when photons from one or more waves are annihilated and new photons are created at different frequencies such that net energy and momentum are conserved during the interaction.

There are two cases or types of FWM:

$$\omega_4 = \omega_1 + \omega_2 + \omega_3$$

$$\omega_4 + \omega_3 = \omega_1 + \omega_2$$

In the first case, three photons combine their energy to generate a new photon. And when the frequencies $\omega_1 = \omega_2 = \omega_3$, the process leads to a phenomenon known as third harmonic generation [40]. In general, it is difficult to satisfy the phase-matching condition for such processes to occur in optical fibers with high efficiencies. However, if $\omega_1 = \omega_2 \neq \omega_3$ it is called frequency conversion. In the second case, two photons of frequency ω_1 and ω_2 are annihilated, while two photons of frequency ω_3 and ω_4 are generated simultaneously. Note that the phase matching condition for this process is $\Delta k = 0$.

In general case in which $\omega_1 \neq \omega_2$, one must launch two pump beams for FWM to occur, however, if $\omega_1 = \omega_2$ single photon can be used to initiate FWM, which is termed Degenerate FWM and this is quite useful for optical fibers. [40]. For instance, a strong pump at frequency ω_1 creates two sidebands located symmetrically at frequencies ω_3 and ω_4. Where ω_3 and ω_4 corresponds to low and high frequency sidebands respectively.

2.3.4 Stimulated Raman Scattering (SRS)

Raman effect was discovered by Raman in 1928 [41], he articulated that Raman scattering can lead to transfer of a small fraction of power (typically on the order $\sim 10^{-6}$) from one optical signal to another, hence, leading to the signal

frequency downshift by certain amount depending on the vibrational modes of the medium [42]. From a practical point of view, the imposed light on the material serves as a pump, which then leads to emission of a frequency modulated light known as Stokes wave, which is indeed a vital spectroscopic tool. Moreover, it can be elucidated from quantum mechanical perspective as energy conversion by a molecule as it makes a transition from an excited virtual state of higher energy to a vibrational state of lower energy as shown in Figure 2.3.

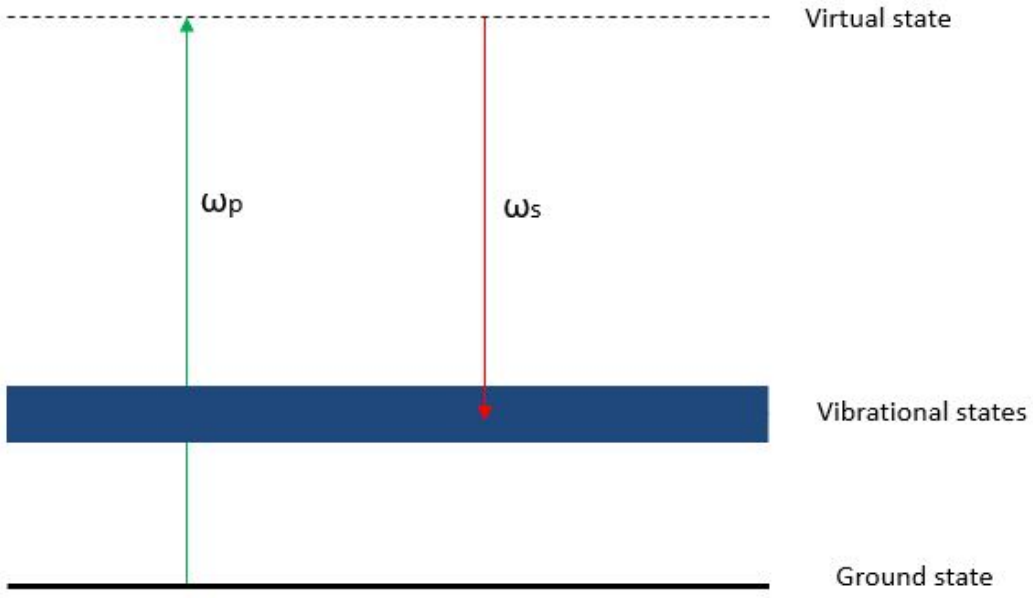

Figure 2.3: Molecule transition. A pump of photon energy $\hbar\omega_p$ excites the molecule to a higher energy level (i.e. virtual state shown by a dashed line). Consequently, a photon of reduced energy $\hbar\omega_s$ is generated as the molecules makes a transition to the vibrational states.

For CW and quasi-CW signals, an expression for the initial growth of the Stokes wave is given by [43]

$$\frac{dI_s}{dz} = g_R I_p I_s \tag{2.72}$$

where I_s is the Stokes intensity, I_p is the pump intensity and g_R (can also be written as Ω) is the Raman gain coefficient, where g_R is related to imaginary part of the third order nonlinear susceptibility. The Raman gain coefficient g_R

can further be explained as the difference in frequency between the pump and Stokes waves, that is $\Omega \equiv \omega_p - \omega_s$, where ω_p and ω_s represents pump and Stokes frequency respectively. In general, Raman gain depends on the core composition as well as the state of polarization of both the pump and Stokes waves.

As pump signal is launched into an optical fiber (assuming CW), the pump power doesn't remain constant upon propagation along the fiber, therefore, equation (2.72) should be modified to include a loss. Also the nonlinear interaction between the pump and stokes should be taken into consideration.

$$\frac{dI_s}{dz} = g_R I_p I_s - \alpha_s I_s \tag{2.73}$$

$$\frac{dI_p}{dz} = -\frac{\omega_p}{\omega_s} g_R I_p I_s - \alpha_p I_p \tag{2.74}$$

Where α_p and α_s stands for fiber losses at the pump and Stokes frequencies respectively.

Although it is absolutely vital to include pump depletion for a complete description of SRS, however, it can be neglected for the purpose of estimating the Raman threshold [42], hence, by neglecting the first term in equation (2.74) and solve for I_p, then by substituting for I_p in (2.73) we get

$$\frac{dI_s}{dz} = g_R I_{p(0)} exp(-\alpha_p z) I_s - \alpha_s I_s \tag{2.75}$$

where $I_p(0)$ is the incident pump intensity at $z = 0$, and the solution to this equation is

$$I_s(L) = I_{s(0)} exp[g_R I_{p(0)} L_{eff} - \alpha_s L] \tag{2.76}$$

L is the fiber length and L_{eff} is the effective length of the fiber. And an expression for the Stokes power is obtained from the above equation as

$$P_{s(L)} = P_{s(0)} exp[g_R I_0 L_{eff} - \alpha_s L] \tag{2.77}$$

The Raman threshold is defined as the input pump power at which the Stokes power becomes equal to the pump power at the fiber output [43] that is

$$P_s(L) = P_p(L) = P_p(0) exp(-\alpha_p L) \tag{2.78}$$

where $P_0 = I_0 A_{eff}$ is the input pump power and A_{eff} is the effective core area. And by assuming $\alpha_P \approx \alpha_s$ the threshold condition becomes:

$$P_{s(0)} exp[g_R P_{p(0)} \frac{L_{eff}}{A_{eff}}] = P_p(0) \tag{2.79}$$

The above equation provides the critical pump power required to reach the Raman threshold. Once the threshold is reached, rapid power transfer from pump to Stokes take place. In fact, in the absence of losses in the fiber, a complete transfer of pump power is expected, according to theoretical predictions. However, in practice, when the power of the generated Stokes wave is large enough to satisfy (2.79), it can serve as a pump, thereby generating second order Stokes wave [43]. Consequently, depending on the input pump power, multiple Stokes wave can be generated due to cascaded SRS.

2.3.5 Stimulated Brillouin Scattering (SBS)

Stimulated Brillouin Scattering (SBS) is a nonlinear phenomena occurring in optical fibers at much lower input power compared to Stimulated Raman Scattering (SRS). Similarly, once the threshold is reached for SBS, Stokes waves are generated whose frequency is downshifted from that of the incident light [44]. However, the generated Stokes wave propagates in backward direction, in contrast to SRS that can occur in both directions. Furthermore, there are several differences between SBS and SRS, SBS seize to occur for short pulses, also its threshold is

determined by the spectral width of the pump signal. As mentioned previously SBS is associated with acoustical phonons whereas SRS is associated with optical phonons.

The acoustic wave produced in SBS leads to change in density of the material, which in turn alters the medium's refractive index. As a result, the pump light scatters via Bragg diffraction due to index grating induced by the pump [45]. Moreover, according to quantum mechanical perspective, such scattering can be viewed as an annihilation of a pump photon which in turn simultaneously generates a Stokes wave and an acoustic phonon.

2.4 Supercontinuum generation in optical fibers

So far we have seen the basic physical phenomena that contributes to spectral broadening in optical fibers, as outlined in the preceding sections of this chapter. Although it is often convenient to describe supercontinuum generation in terms of the group velocity dispersion regimes, namely normal and anomalous dispersion regimes. However, supercontinuum generation is much more complicated than that, hence, pulse parameters also plays an extremely important role when it comes to spectral broadening. The goal of this section is to give a further insight on some of the phenomena or interactions discussed in the preceding sections in order to elucidate the commonly observed features of fibre supercontinuum generation.

Herein, we consider two possible pump regimes in which the supercontinuum generation is clearly distinguished, these are the short (i.e. femtosecond) and long (i.e. nanosecond, picosecond and continuous wave) pump pulses [46].

2.4.1 Supercontinuum generation in short pulse regime

To have a better insight of supercontinuum generation in the short pulse regime, it is crucial to consider the case of pumping in the anomalous dispersion regime close to the zero dispersion wavelength. Under typical pumping conditions, the power of the pump pulses is high enough for the input pulses to be considered as solitons of order $N >> 1$ which is referred to as higher order soliton. However, the incident pulses undergo perturbation due to some physical effects such as higher order dispersion, self steepening and stimulated raman scattering, which leads to breaking up of the higher order soliton into fundamental solitons, and this phenomenon is referred to as SOLITON FISSION [47]. Once soliton fission occured, energy of the solitons ejected from the higher order soliton is shed through generation of dispersive waves in the normal dispersion regime. Consequently, such dispersive wave components are responsible for spectral broadening in the short wavelength regime. While further spectral broadening in the long wavelength regime is attributed to Raman soliton self-frequency shift, and in some cases, cross-phase modulation between dispersive waves and Raman solitons.

Observation of such processes is not apparent via simply measuring the spectrum at the fibre output, however, manifestation of such processes is quite feasible via numerical modelling. Below in Figure 2.4 we have a very good example of a numerical result illustrating both the effects of soliton fission as well as dispersive waves generation.

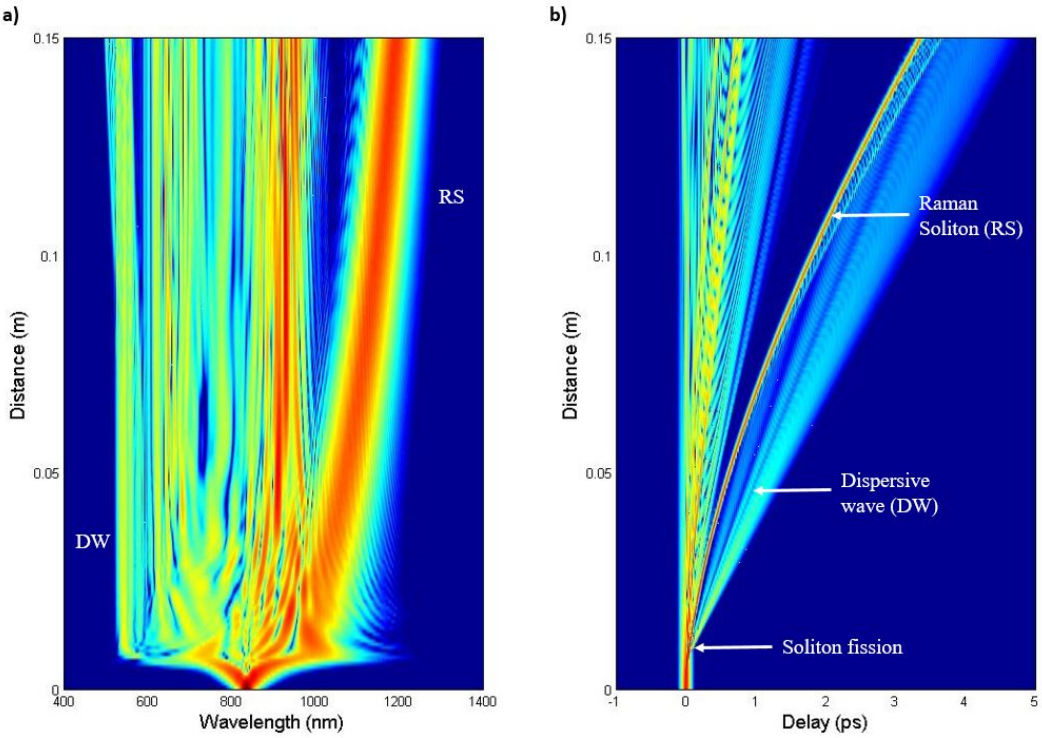

Figure 2.4: a) and b) density plot representations of supercontinuum generation in the femtosecond regime in spectral and time domain respectively. The plots highlight the point of soliton fission, the characteristic features of dispersive wave radiation, and the frequency and time-domain evolution of an ejected soliton undergoing the Raman soliton self-frequency shift.

These simulations correspond to the case of pumping in the anomalous dispersion regime of a PCF with a secant hyperbolic pump pulses of $50fs$ duration (FWHM) and $10kW$ peak power at $835nm$ in a PCF with zero dispersion wavelength around $780nm$ [46].

We can also define a characteristic length scale to describe the point at which the soliton fission starts or takes place, which is coined fission length and is given by $L_{fiss} \approx L_D/N = \sqrt{L_D L_{NL}}$. Approximately after such a propagation distance, the split of the initial pulse begins.

So far we have assumed the input pulse is propagating in the anomalous dispersion regime, in the case of propagation in the normal dispersion regime the initial spectral broadening is mainly due to self phase modulation. However, for

pumping in the normal regime but near the zero dispersion wavelength (ZDW), again the initial broadening is by SPM, but in this case some of the spectral contents are tranfered into the vicinity of the ZDW and into the anomalous regime, and once this happens, a spectral broadening similar to that of pumping in the anomalous regime takes place [46].

2.4.2 Supercontinuum generation in long pulse regime

For long pump pulses in the anomalous dispersion regime, the soliton order becomes very large (i.e. $N >> 10$), hence soliton fission becomes less important, because the characteristic fission length required for soliton fission to occur scales with pump pulse duration. Therefore, at the initial propagation stage, the dominant contribution is by spontaneous modulation instability (MI) and four wave mixing (FWM). Under these conditions, the input pulse breaks into multiple sub-pulses in the temporal domain. The subsequent evolution of these sub-pulses leads to spectral broadening, hence supercontinuum generation via several mechanisms such as dispersive wave generation and Raman self frequency shift. For pumping with long pulses in the normal dispersion regime, the initial spectral broadening is attributed to four wave mixing and Raman scattering.

2.5 Numerical modelling

Generally, there isn't any analytical solution to the nonlinear schrodinger equation (NLSE), even numerical solutions to NLSE are hard to implement due to dimensionality of the problem. Therefore in order to have an approximate solution to the scalar form of the NLSE, approximations based on experimental results and propagation conditions are extremely crucial.

This section aims at familiarizing us with one of the most powerful technique in numerically solving the NLSE, known as the split-step Fourier method (SSFM).

The SSFM happens to be most preferable technique due to its easy implementation and speed compared to other numerical techniques such as finite difference time domain (FDTD). SSFM provides solution using pseudo-spectral methods whereas finite difference method solves the Maxwell's wave equation in time domain (using the assumption of paraxial approximation) which is slower by an order of magnitude compared to SSFM [48]. Another significant distinction between finite difference methods and SSFM is that, the former can account for both forward and backward propagating waves, because it deals with all the electromagnetic components. However, the NLSE in the latter just deals with forward propagating waves. Hence, it is quite apparent that the SSFM works efficiently and accurately for describing pulse propagation in microstructured fibers.

2.5.1 Split-step Fourier method (SSFM)

$$\frac{\partial a}{\partial z} = [-\frac{\alpha}{2} - \sum_{m=2} \frac{i^{m-1}}{2^{m-1}} \beta_m \frac{\partial^m}{\partial t^m}]a + i\gamma[|a|^2 + \frac{i}{\omega_0 a} \frac{\partial |a|^2 a}{\partial t}]a - T_R \frac{\partial |a|^2}{\partial t} a \qquad (2.80)$$

The above equation is referred to as Generalized nonlinear Schrodinger equation (GNLSE), where the first part on the right represents dispersion and losses, the second part represents nonlinearity and the third part represents Raman effects. The split-step Fourier method as the name implies, is an iterative process which presents a simple solution to the NLSE by propagating the pulse envelope for small distances step by step throughout the entire length of the fiber.

Equation (2.80) above can be represented with two distinct operators $\hat{D}$ and $\hat{N}$ which stands for dispersion(including loss) and nonlinear operators respectively [48].

$$\hat{D} = -\frac{\alpha}{2} - \sum_{m=2} \frac{i^{m-1}}{2^{m-1}} \beta_m \frac{\partial^m}{\partial t^m}$$

$$\hat{N} = i\gamma[|a|^2 + \frac{i}{\omega_0 a} \frac{\partial |a|^2 a}{\partial t} - T_R \frac{\partial |a|^2}{\partial t}]$$

Now the GNLSE takes the form

$$\frac{\partial a(z,t)}{\partial z} = (\hat{D} + \hat{N})a(z,t) \tag{2.81}$$

Since the SSFM is an iterative process, therefore solution to the NLSE at any step h of the fiber/waveguide becomes

$$a(jh,t) = exp[\hat{D} + \hat{N}]a((j-1)h,t) \tag{2.82}$$

where j is an integer ($j = 1, 2, ...$). Note that the operator $\hat{N}$ multiplies the field solution $a(z,t)$ whereas the operator $\hat{D}$ is a differential that operates on $a(z,t)$, hence complicates and requires more time for simulation. For the sake of simplicity, by taking Fourier transform of the operator $\hat{D}$, the derivatives in time domain transforms into multiplication in the frequency domain thereby minimizing computational time. The operator $\hat{D}$ then becomes

$$\hat{D}(i\omega) \equiv \mathscr{F}[-\frac{\alpha}{2} - \sum_{m=2} \frac{i^{m-1}}{2^{m-1}}\beta_m \frac{\partial^m}{\partial t^m}] = -\frac{\alpha}{2} - \sum_{m=2} \beta_m \frac{i^{m-1}}{2^{m-1}}(i\omega)^m$$

The solution to the propagating pulse envelope $A(z,t)$ per spatial step h at step jh for the entire fiber length is given by the expression

$$a(jh,t) \approx \mathscr{F}^{-1}[exp(h\hat{D}(i\omega))\mathscr{F}[exp(h\hat{N})a((j-1)h,t)]] \tag{2.83}$$

The corresponding procedure during each single step is illustrated in the figure below :

As can be seen from figure (2.5) the incident pulse $a(0,t)$ enters the fiber of length L at $z = (j-1)h$. The length L is split into $S_L = L/h$ steps of length h. The nonlinearity is calculated at step midpoint 1 while dispersion is calculated at point 2 ($z = jh$) that is over step h in the frequency domain. The iterations are repeated until the fiber length L in order to obtain a corresponding final solution at the fiber end.

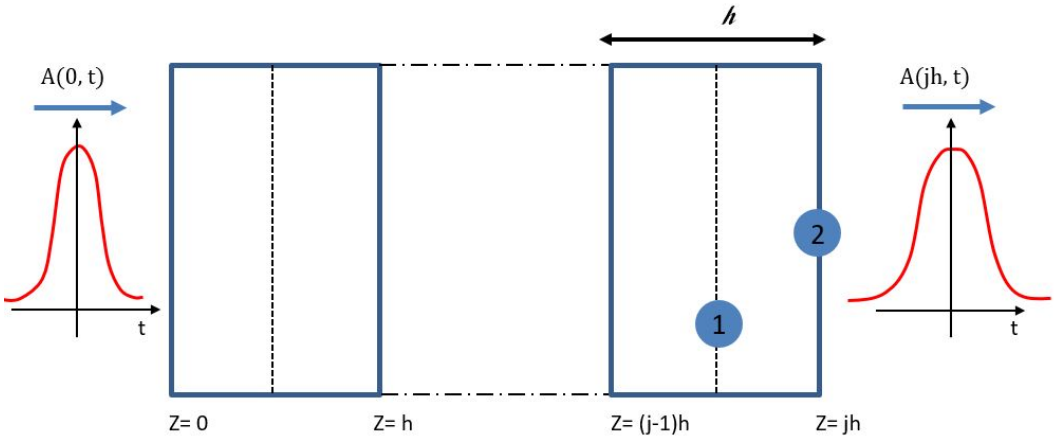

Figure 2.5: The SSFM for a single iteration of step h starting at z=(j-1)h.

2.5.2 Windowing and sampling (temporal/spectral)

Fast Fourier transform (FFT) provides a robust approach for computing Fourier transforms, however, it does pose restrictions on the sample array format [48]. Therefore, number of points $N = 2^m$ is absolutely critical for FFT of a sample array $a(z,t)$ for each value of z. It is also crucial that the starting array $a(0,t)$ samples the initial pulse with same intensity and phase, also sufficient temporal width and resolution are absolutely vital in order to prevent wrapping and aliasing errors. Hence, proper diligence is required when deciding the format, length, and resolution of the complex array. Adequate sampling rate can be determined by Nyquist theorem, which states that the minimum sample frequency is twice the highest frequency sinusoidal component of significant amplitude.

For an accurate sampling using the SSFM, one has to chose a temporal resolution $\delta t = 1/(2*4*\Delta\nu)$ (where ν represents spectral width), such that the total temporal window $N * \delta t$ will be at least twice the final pulse temporal FWHM (Δt) at $z = L$. Similarly, the corresponding spectral resolution should be determined by $\delta\nu = 1/N * \delta t$. Then determine if the corresponding spectral window $N * \delta\nu$ will be at least twice the final spectral FWHM ($\Delta\nu$) at $z = L$. Finally, the choice for the value of N is at the expense of the computation time, hence reasonable value for N should be chosen for a better result.

2.5.3 Spatial step size

The spatial step size h for the SSFM can be chosen by first computing the dispersion length L_D and nolinear lenght L_{NL} (which are well discussed in chapter2) to the fiber length L. For situations where, $L_D \ll L \ll L_{NL}$ or $L_{NL} \ll L \ll L_D$, the NLSE can be solved analytically as discussed in the preceding chapter. If L is comparable to L_D and L_{NL}, a smaller value for h can be chosen. A value for h should be chosen such that $\lambda_0 < h < L_D$ and $\lambda_0 < h < L_{NL}$. The step-size should be considerably smaller than both L_D and L_{NL} for the solution via the SSFM to be meaningful. It is also important to compute the spectral energy before and after propagation, again h can be made small if the energies are not approximately equal.

2.5.4 Errors associated with SSFM

So far we have seen the necessity for proper choice of step-size and temporal/spectral windowing which are bound to the Nyquist theorem. It became clear that a wrong choice of temporal/spectral windowing may lead to certain errors, such as aliasing and wrapping error, while a wrong choice of step-size can leads to spectral energy not being conserved [48].

Chapter 3

Direct tapering of chalcogenide materials for nonlinear applications

Conventionally, a tapered fiber can be produced by cautiously stretching an optical fiber while being heated, such that the fiber becomes soft. This process leads to a decrease in the fiber diameter over some length. Consequently, the fiber core diameter also decreases by the same factor as the total fiber [49].

Due to substantial low melting temperature of chalcogenide glasses ($\sim$ 300 C), open flame tapering system can not be used. Therefore tapering chalcogenide glasses has to be carried out via resistive heating or via any sort of controlled heating system, that can melt chalcogenide glasses without evaporating it. Another complication arises when tapering step index chalcogenide core/cladding fibers, where chalcogenide compositions are highly susceptible to interdiffussion of the core and cladding material and volatilization of the glass constituents at elevated temperatures [50].

Fiber tapering have been an important practical aspect of photonics, for instance, silica nanowires with sub-wavelength diameters were made from bulk

silica fiber [51], which are crucial for various photonics applications such as absorption spectroscopy [52], sensing [53]. Also, tapered sub-micron chalcogenide fibers were shown to exhibit an ultrahigh nonlinearity which in turn minimizes the supercontinuum generation input power threshold [54].

Herein, we developed a unique technique of fabricating nanowires/sub-micron fibers directly from bulk chalcogenide materials which we referred to as "Direct tapering". Furthermore, this direct tapering technique mitigates some of the outlined challenges associated with tapering chalcogenide glasses. In the following sections/subsections, we will be discussing; the fabrication steps, advantages of the technique compared to conventional fiber tapering process, demonstration of supercontinuum generation using the technique, and some of the important results obtained.

3.1 Fabrication steps

3.1.1 Silica fiber tapering

Firstly, the conventional open flame tapering system was used to taper a silica fiber (which comprises of a germanium doped core, cladding and a polymer jacket). Indeed before tapering the fiber, polymer jacket at the region to be tapered was removed by simple stripping using a fiber stripper. The stripped region of the fiber was cleaned with methanol to avoid any sort of contamination that may temper with the tapering process. The fiber was then mounted upon a motorized translating stage/clamp (Newport. Universal Motion Controller(Model ESP300)/MFA-CC) and held firmly. A continuous wave(CW) laser source (Santec TLS-510) was butt coupled to the fiber at one end and the other end was butt coupled to a power meter (Newport 1935C) in order to observe the power transmission while tapering (as shown in figure 3.1.a)). A flame from a hydrogen torch was placed right at the center just beneath the mounted stripped silica fiber as shown in 3.1.b). After about 60 - 80 seconds of heating, a tilt in the

firmly mounted fiber was observed. Tapering was immediately initiated using a customized software, and the corresponding power transmission was recorded in-situ. From the transmission spectrum one can be able to distinguish between a lossy and an adiabatic tapering as shown in figure 3.1.c).

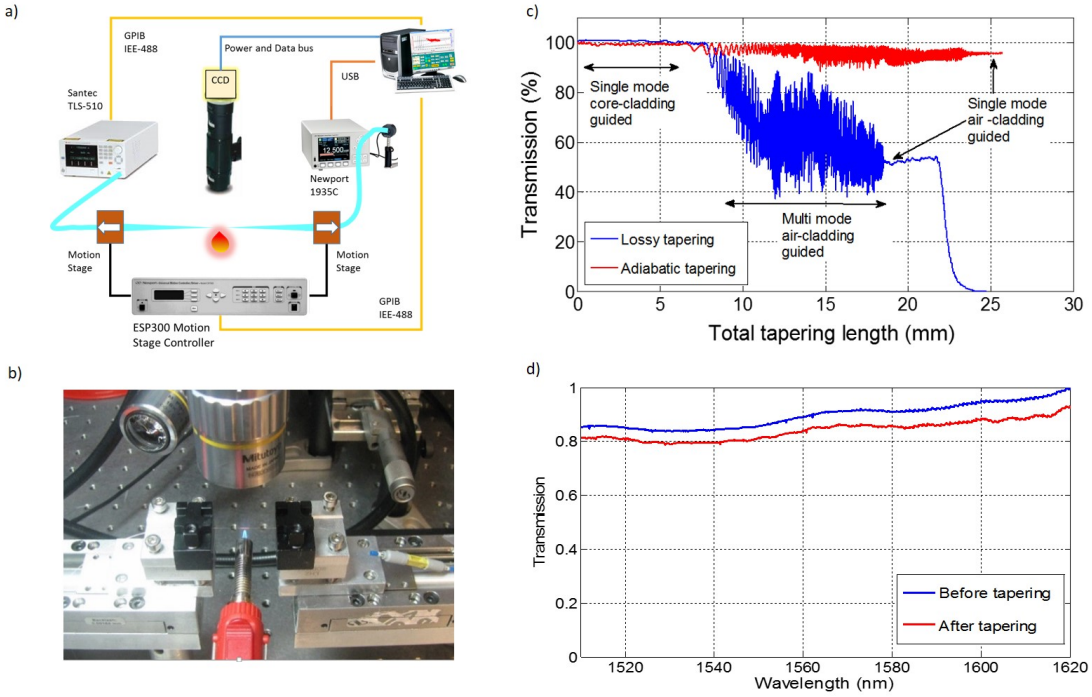

Figure 3.1: (a) shows a schematic representation of our setup for silica fiber tapering, (b)is a picture of the tapering part of the setup, (c) shows the power transmission against tapering length of the silica fiber and (d) compares the power transmission before and after tapering.

Initially, the fiber comprises of a single mode core-cladding guided light. However, upon tapering down to certain diameters, the core eventually disappeared leaving a multi mode air-clad silica fiber (remember as mentioned earlier the core diameter of a tapered fiber decreases by the same amount as the whole fiber). After some further tapering, a single mode air-cladding guided fiber was obtained. Figure 3.1.d) shows the difference in transmission before and after tapering. It can be clearly seen that an adiabatic low loss tapering was successfully obtained.

3.1.2 Direct tapering of chalcogenide materials

After a successful adiabatic tapering of the silica fiber (with an air-cladding guided single mode), using a blade (Ideal DualScribe S90R) placed right at the center of the tapered silica fiber, the fiber was precisely cleaved under a microscope into approximately two equal halves. The successfully cleaved silica fibers were pulled apart using the motorized stage(Figure 3.2 a) 2) to provide enough space for chalcogenide feeding. Using a setup as shown in Figure 3.2 a), bulk chalcogenide on a glass slide was placed right in between the cleaved fibers (Figure 3.2 a) 4 and 5), both the cleaved fbers and the bulk chalcogenide were enclosed by a homemade electrical heater (Figure 3.2 a) 1), which provides enough heat to melt the bulk chalcogenide glass.

Figure (3.2, b)) is the home made electrical heater used for melting chalcogenide glasses. And c) shows the corresponding temperature variation as a function of voltage. The heater was customized to have a saturation at 140 V, where any further increase in voltage will be automatically limited to the melting temperature of the chalcogenide materials.

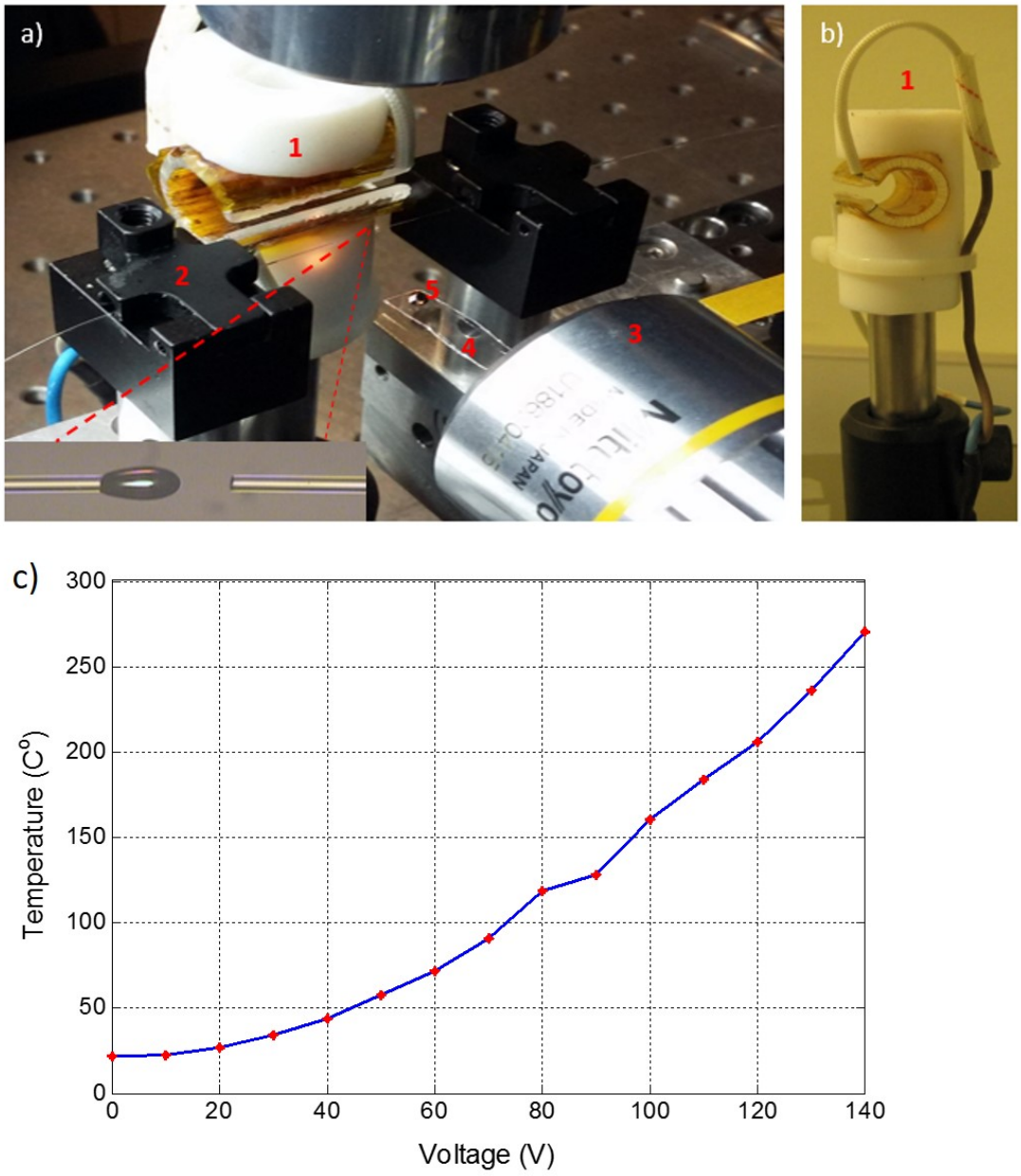

Figure 3.2: a) Shows the setup used for direct tapering of chalcogenide materials, where 1 is the home made electrical heater, 2 is the motorized stage/clamp upon which the silica fiber was mounted and held firmly on either sides, 3 is a microscope for insitu observation of the tapering process, 4 is a glass slide for chalcogenide feeding and 5 is the bulk chalcogenide. b) 1 is the home made electrical heater which was used to melt the chalcogenide glasses and c) shows the corresponding temperature of the homemade electrical heater at certain voltages.

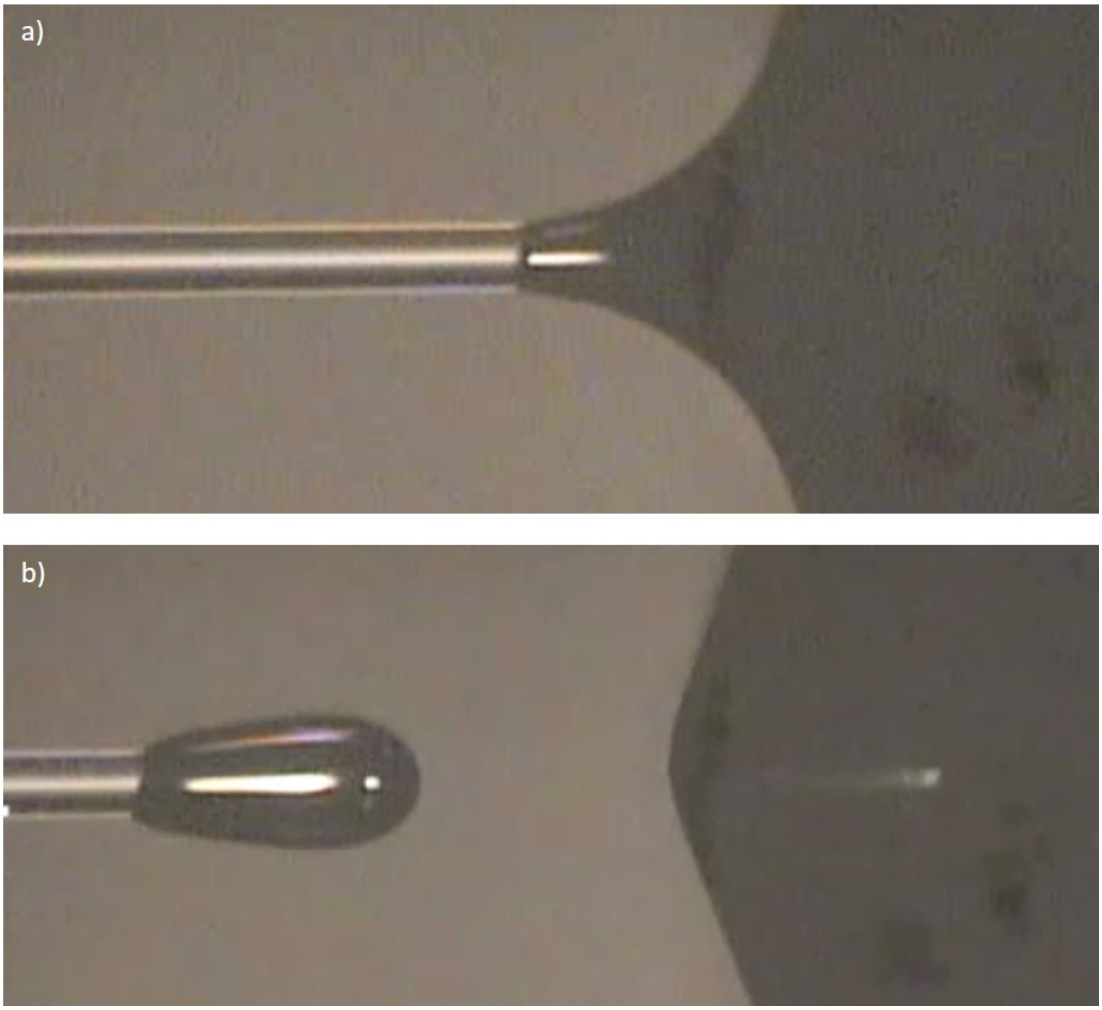

Figure 3.3: a) and b) shows the initial feeding of molten chalcogenide upon the tip of tapered silica fiber.

After we have everything set as discussed, we then turn on the homemade electrical heater and wait for a couple of minutes for the chalcogenide to melt. Once chalcogenide is in the molten state, it can be transferred to both tips of the cleaved tapered silica fibers, by simply dipping the tapered silica tips one at a time into the molten chalcogenide and pulling it (as shown in Figure 3.3 a) and b)).

By bringing both chalcogenide fed tips into contact with each other, the molten chalcogenide at the two tips merges (Figure 3.4 a)). At this moment, we wait a little while for the chalcogenide to have a smooth distribution and stabilise

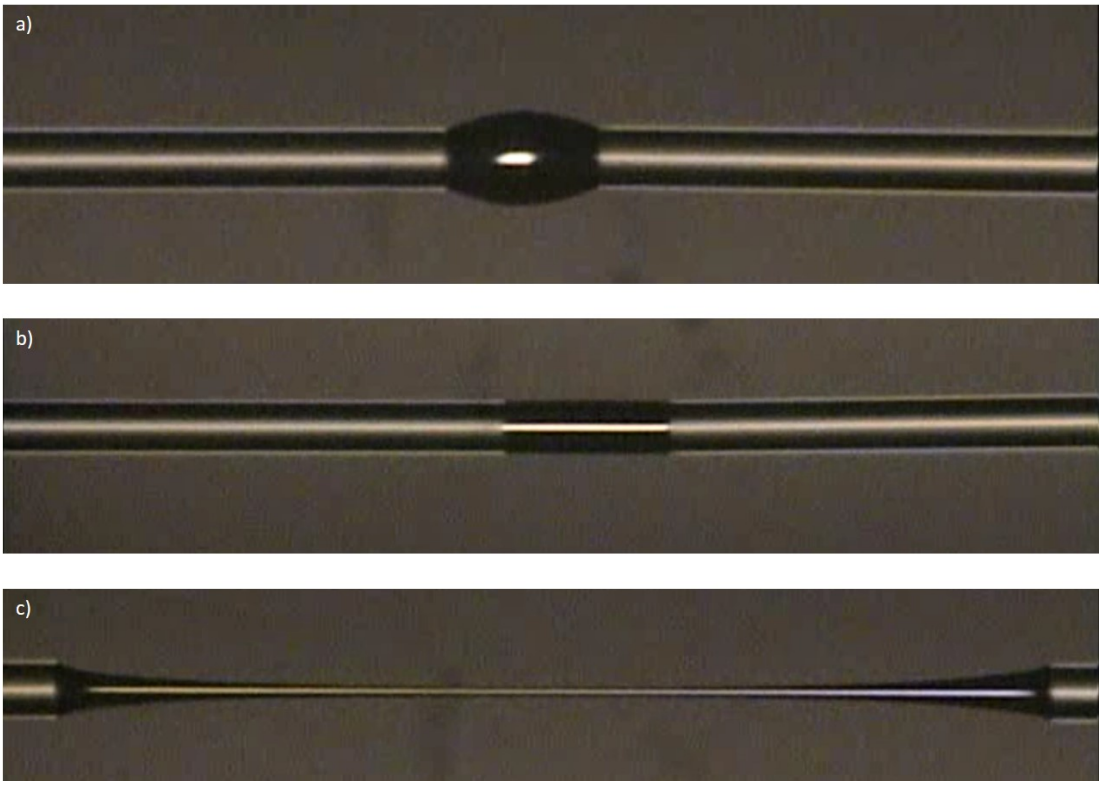

Figure 3.4: a) shows chalcogenide fed between the two tips of the tapered silica fiber by simply bringing both tips into contact. b) A smooth distribution and stabilization of chalcogenide between the tips and c) tapering begins by simply pulling the fibers apart.

between the tips (Figure 3.4 b)). Once that is achieved, we begin tapering of chalcogenide by cautiously pulling it apart using the motorized stage(Figure 3.4 c)).

3.1.3 Results and discussion

Chalcogenide materials (As_2Se_3 and As_2S_3) were successfully tapered adiabatically with tapered waist diameter as low as sub-micron as shown in Figure 3.5. a) and b) shows an adiabatically tapered chalcogenide fibers, and c) shows sub micron diameter adiabatically tapered chalcogenide fiber. This strongly demonstrates the remarkable ability of the technique to directly fabricate nanowires/nanofibers from a bulk material.

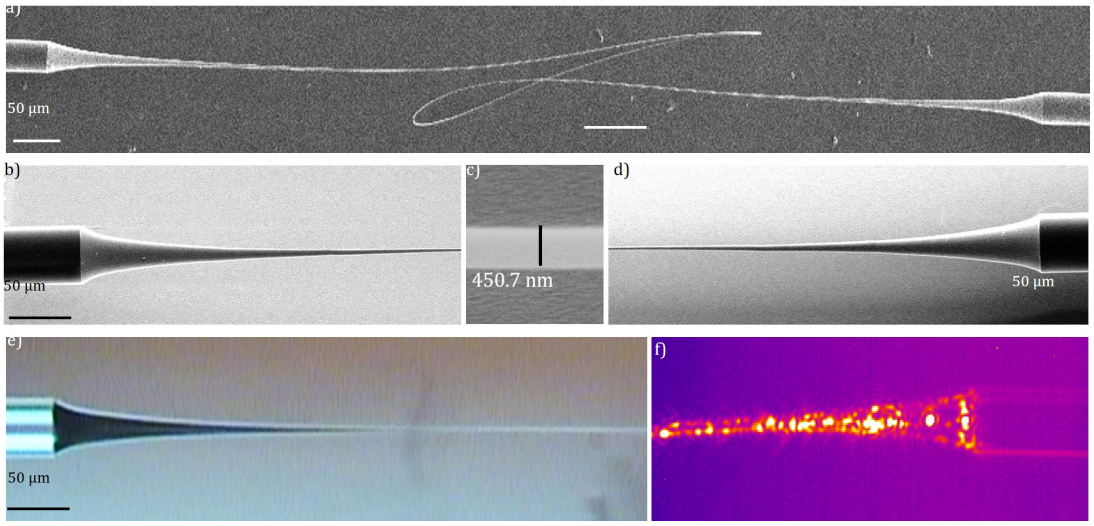

Figure 3.5: a), b) and d)shows an adiabatically tapered chalcogenide fibers. c) Sub micron diameter adiabatically tapered chalcogenide fiber, e) and f) are the corresponding optical microscopic image and thermal camera image.

We obtained a broadband transmission for the tapered ChG fiber (as shown in Figure 3.6), which was drawn until we reached single mode regime at a nanoscale waist diameter. Figure 3.7 compares the transmission spectrum of silica fiber before and after tapering, and that of tapered chalcogenide fiber. The total insertion loss was 21.1 dB, which was the sum of 6.4 dB silica to silica mechanical coupling and propagation loss, 0.6 dB silica fiber tapering loss, 1 dB Fresnel loss for both ChG/silica interface, 9.1 dB ChG tapering loss, and 4 dB loss due to cleaving and mode mismatch. Most of the loss ($\sim$ 14.1 dB) was caused by the processes after silica fiber tapering, which was observed to be at least 8 dB for the best case. Starting ChG fiber tapering with smaller diameter silica tips ($D < 20\mu m$) is more favorable for adiabatic transition of the cladding guided modes, and reducing mode mismatch. The ChG fiber tapering loss includes losses due to nonadiabaticity, surface scattering, and Rayleigh scattering due to density fluctuations caused by different evaporating rates for As and Se, changing stoichiometry of the glass. In principle, angle cleaved silica fiber tips can eliminate the Fresnel losses, and tapering under inert gas atmosphere can reduce oxidation effects degrading ChGs.

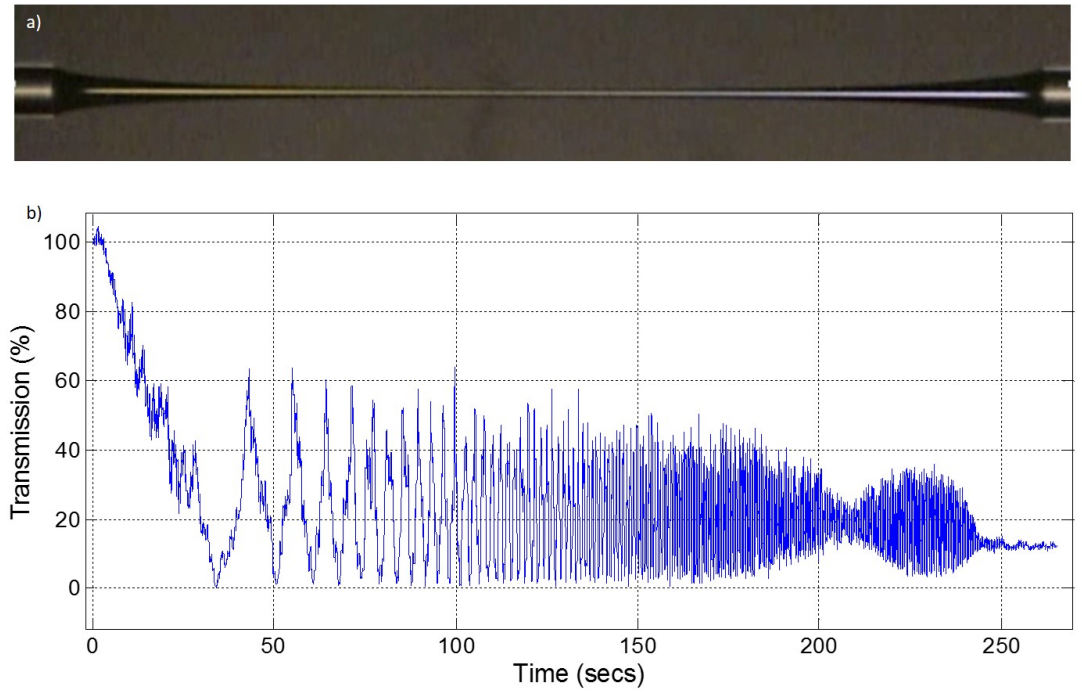

Figure 3.6: a) shows chalcogenide tapering in progress, while b) is the corresponding transmission during the tapering process.

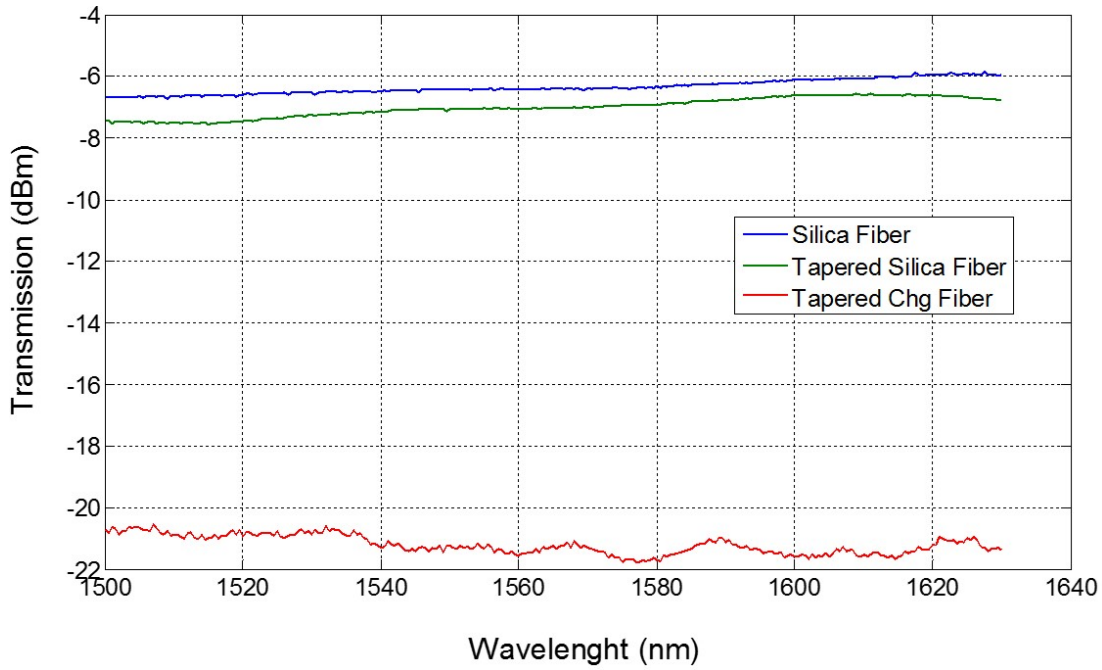

Figure 3.7: Transmission spectrum of silica fiber before and after tapering and that of tapered chalcogenide fiber

One of the major unique advantage of this technique is that an undesired tapered chalcogenide fiber can be remelted (using the home made electrical heater) and retapered several times until a desired tapering is achieved. However, it is important to mention that too much remelting is not advisable because after certain number of remelting, the chalcogenide glass crystallizes due to thermal effects. Another important advantage is that the technique is simple, also nanowires/nanofibers can be fabricated directly from a bulk material which minimizes the number steps and complications compared to other conventional techniques. Although we have used this technique with chalcogenide materials (namely arsenic selenide and arsenic sulphide), other glasses with thermal and mechanical properties compatible with the technique can also be used.

Such tapered chalcogenide fibers are proposed for various applications such as evanescent couplers for critical coupling of light into micro resonators of high refractive index [55], supercontinuum generation, e.t.c. However, in this thesis our focus will be on supercontinuum generation.

3.2 Supercontinuum generation

Certain input power threshold is extremely crucial for supercontinuum generation, as discussed earlier in chapter 2, the nonlinear process itself is an intensity dependent phenomenon. The input power threshold for supercontinuum generation can be minimized by simply tapering an optical fiber. In this section we will demonstrate supercontinuum generation via direct tapering of chalcogenide fibers (mainly As_2Se_3 and As_2S_3) with extremely low input power. Pulse characterization, third harmonic generation (THG) as well as some other results obtained will be discussed.

3.2.1 Pulse characterization

Pulse characterization is absolutely vital for supercontinuum generation, since pulse parameters dictates supercontinuum generation. The femto second laser source used in our experiment was FemtoFiber smart TOPTICA photonics whose pulse was not transform limited and was positively chirped. Moreover, considering our case where we have an air-clad tapered silica fiber (in the normal dispersion regime) connected to the femto second laser source, will indeed lead to further temporal broadening of the pulse, thereby decreasing the input power. And this may perhaps undermine spectral broadening, therefore, to solve this problem, a dispersion compensation is required for the positively chirped pulse. Figure 3.8 represents temporal distribution of the femtosecond laser pulse. As can be seen, the pulse is extremely broad, with $\sim$ 2 ps FWHM. To compensate for such chirping, a long fiber with 125 μm diameter silica cladding and a silica germanium doped core of $\sim$ 8.5 μm in diameter which falls in the anomalous dispersion regime, was butt coupled to the femtosecond laser. Note that negative chirping exists in this regime. As a result, neagtive and positive chirping cancels each other, and this yields dispersion compensation.

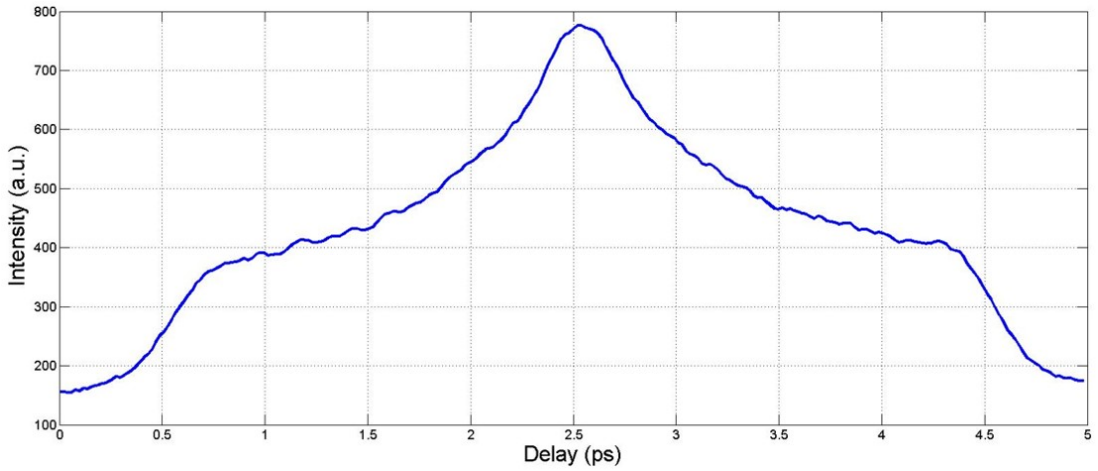

Figure 3.8: Temporal distribution of the positively chirped ultrashort pulse.

At first, the butt coupled fiber that was meant for compensation was extremely long, as a result, arbitrary pulse shapes were observed in the autocorrelation trace. However, by reducing the fiber length while observing the autocorrelation trace

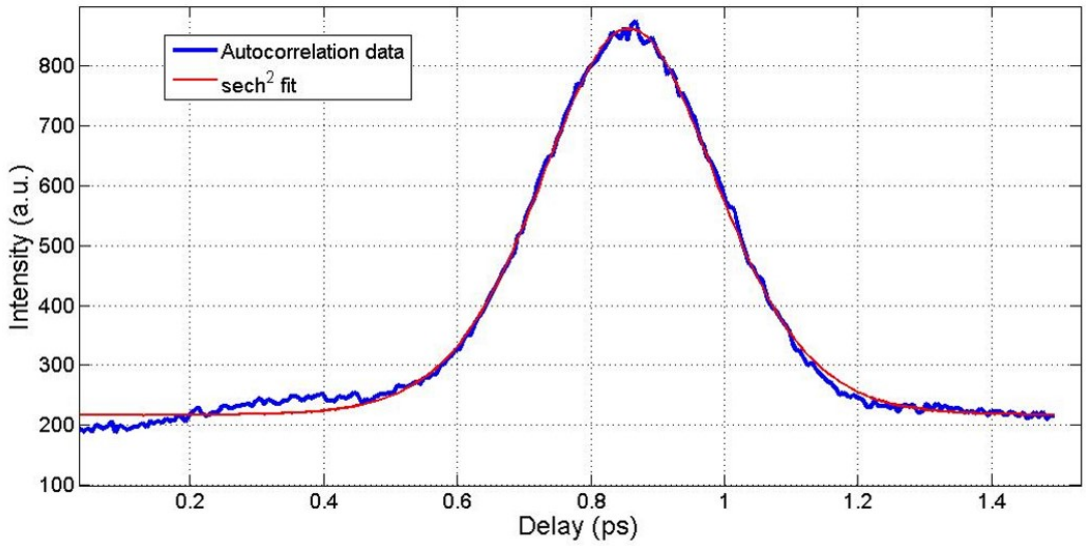

Figure 3.9: Autocorrelation trace data of the chirping compensated pulse. Where blue is the autocorrelation trace data while red is the secant hyperbolic fit.

of the pulse, upon reaching a fiber length of about 5 m - 6 m, a nearly transform limited pulse was obtained as shown in Figure 4.9.As can be seen in figure 3.9, after chirping/dispersion compensation, a nearly secant hyperbolic pulse with $\sim$ 250 fs FWHM was obtained. And one can see that the broad nature of the initial pulse no longer exists, thus, compensation is verified. Vehemently, this pulse is good enough for supercontinuum generation.

3.2.2 Demonstration

In this subsection, demonstration of supercontinuum generation in both As_2Se_3 and As_2S_3, third harmonic generation and other observed effects will be discussed.

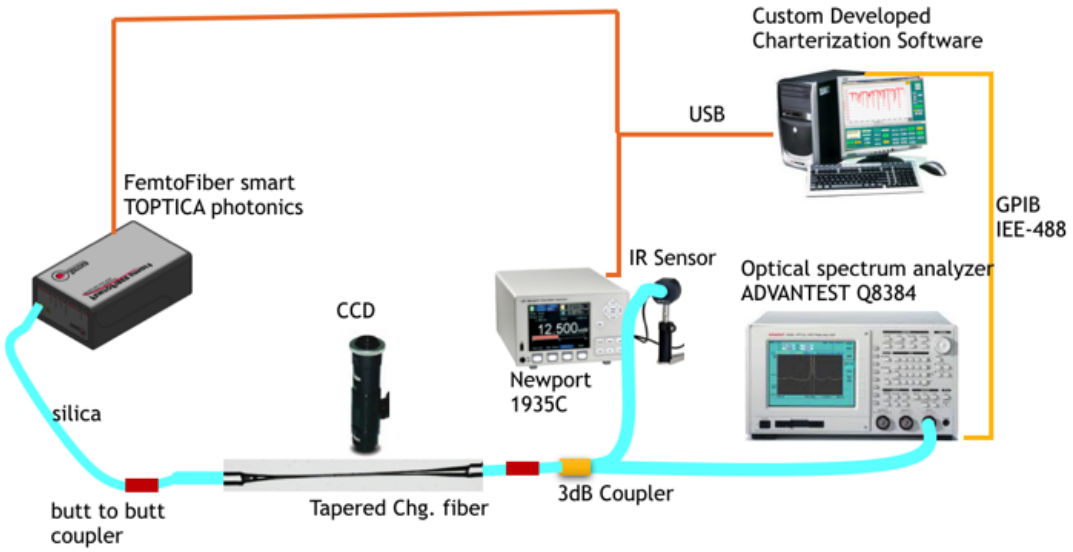

Figure 3.10: Setup for supercontinuum generation in directly tapered chalcogenide fibers.

Figure 3.10 was the setup used for supercontinuum generation in tapered chalcogenide fibers. As can be seen, the setup is similar to that of figure 4.1a, just that the CW laser system was replaced with a femtosecond laser system, also an optical spectrum analyzer (OSA) was used to observe the output spectrum.

Chalcogenide fibers were tapered via the direct tapering technique (as discussed in section 3.1.2). A pump pulse as described in Figure 3.9, which has a center wavelength around 1560 nm, a pulse width (FWHM) of $\sim$ 250 fs, repetition rate of 100 MHz and an average output power of $\sim$ 100 mW was used. Although light was successfully coupled into the tapered chalcogenide fibers, it is however important to mention that only few hundreds μW was successfully coupled into the tapered fiber. The tremendous amount of power loss recorded was attributed to losses such as, losses arising from butt coupling of silica fiber to the femtosecond laser device, losses due to tapering of both silica and chalcogenide

(as shown in Figure 3.7), losses arising from butt to butt coupler (which leads to $\sim$ % 50 drop in power from each butt to butt coupler), also Fresnel losses at the interfaces between silica and chalcogenide fibers.

3.2.3 Results and Discussion

Interestingly, when light was coupled into the tapered chalcogenide fibers, a visible green light was observed. Moreover, even after the fiber was splitted green light still appeared at the fiber tip, both cases are shown in figure 3.11 a) and b). Considering the fact that green light in the visible spectrum falls between approximately 510 - 570 nm, and our pump has a center wavelength around 1560 nm, we then suggested that the observed green light was due to non-phase matched third harmonic generation.

Unfortunately, the lowest wavelength that can be recorded by our OSA is around 600 nm, which is far away from green region in the visible spectrum. And for this reason we could not observe a third harmonic generation peak in the OSA. However, in order to verify our claim that the observed green light was indeed due to third harmonic generation (THG), we coupled the green light into a Maya visible spectrometer and observed the spectrum.

As can be seen from figure 3.12 the peak is exactly at 520 nm, this clearly verifies our claim that indeed the observed green light was due to non-phase matched third harmonic generation. Note that this was observed in SCG with both As_2Se_3 and As_2S_3.

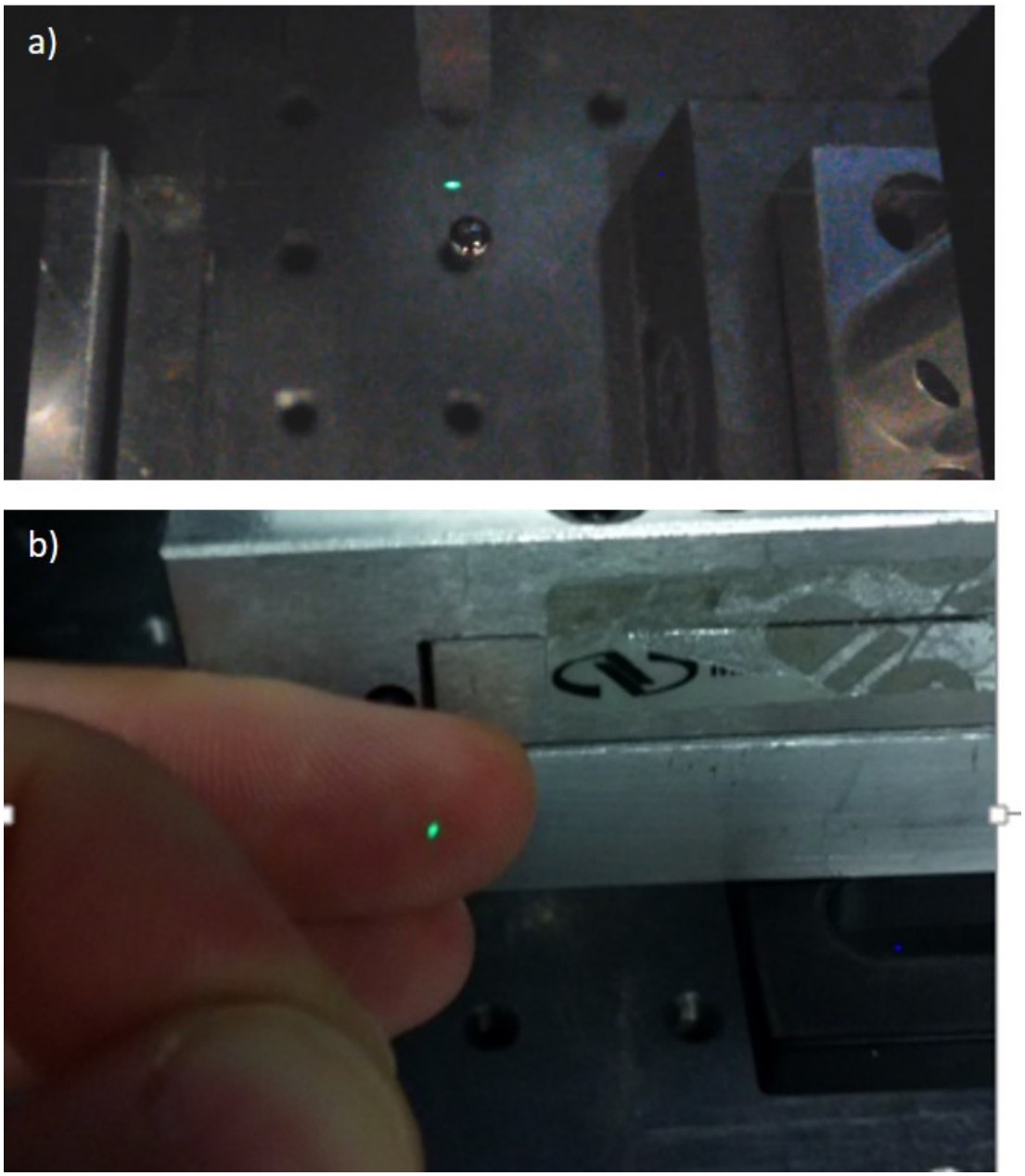

Figure 3.11: a) Visible green light observed during SCG process in the fiber before tapered chalcogenide fiber got splitted, b) and at the fiber tip after it got splitted.

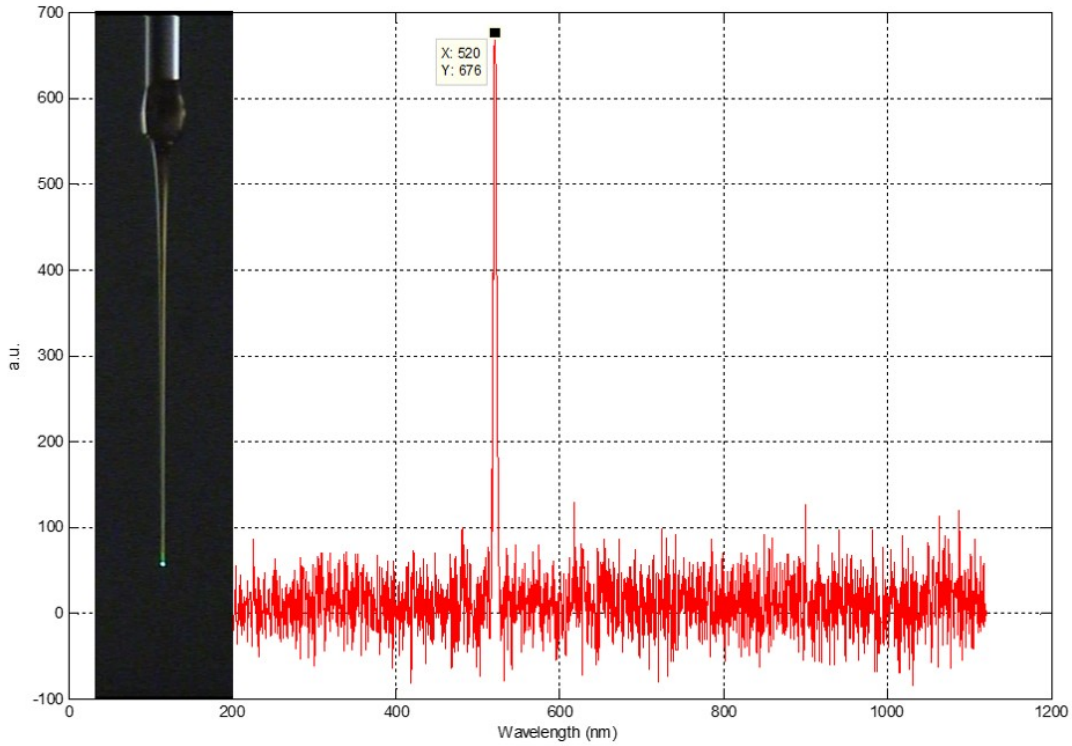

Figure 3.12: Ouput spectrum from a Maya visible spectrometer with a peak at exactly 520 nm wavelength.

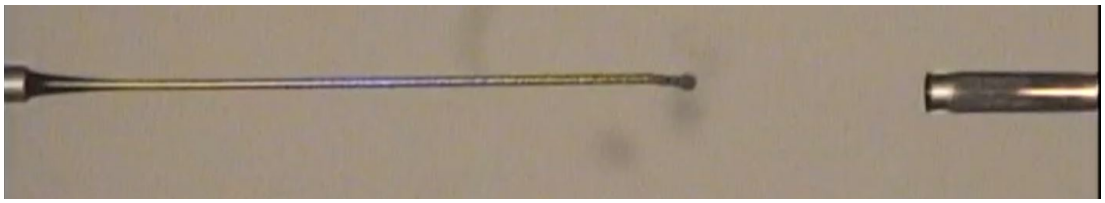

Figure 3.13: As_2Se_3 evoporation via absorption of 520 nm wavelength THG.

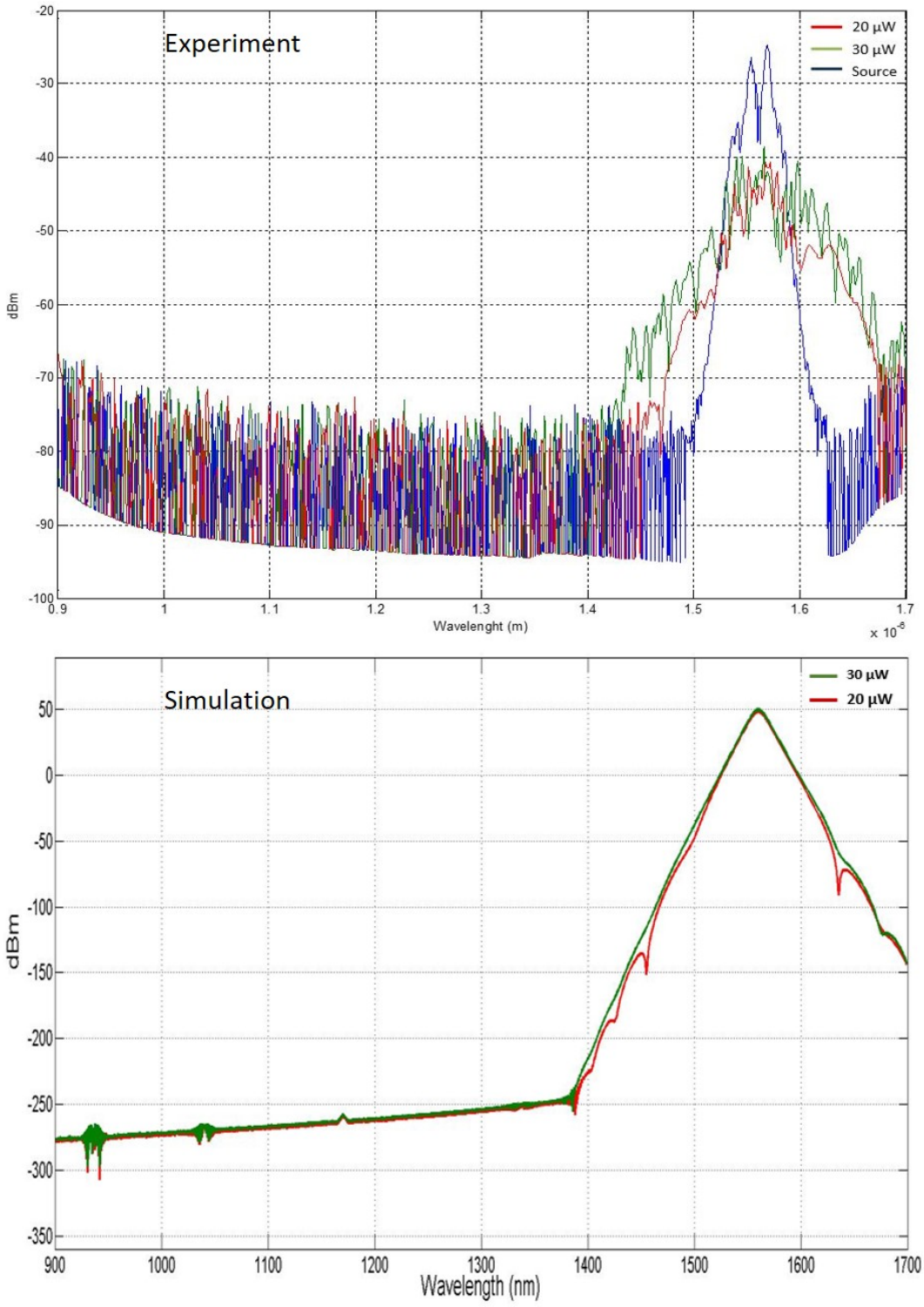

Figure 3.14: Experimental and numerical data showing output spectrum for SCG in As_2Se_3 at different average power levels, where blue is the incident pulse spectrum, red and green are the output spectrum at 20 μW and 30 μW respectively.

Figure 3.14 shows both numerical and experimental output spectra for SCG in As_2Se_3, where red and green are the output spectrum at 20μW and 30 μW input average power respectively. The simulation was carried out via split-step Fourier method, using a secant hyperbolic pulse of pulse duration τ_0 = 142 fs at λ_0 = 1560 nm, β_2 = -1.01 ps^2m , γ = 23.2 $W^{-1}m^{-1}$ and a fiber length of l = 2.5 mm. Apparently, a good agreement between experiment and simulation is shown. As can be seen, a broadening of about 300 nm - 400 nm was observed with an average pump power as low as 30 μW (which corresponds to a peak power of $\sim$ 2 W). Enough average power was not able to be coupled into the tapered As_2Se_3 due to two reasons. The first reason was mentioned previously, which is due to tremendous amount of insertion losses. The second reason is due to high absorption of 520 nm ligt generated due to THG in As_2Se_3. Where at high average input powers, As_2Se_3 suddenly evaporates (Figure 3.13). That is why we always introduce an additional bending loss to the silica fiber butt coupled to the ultrafast laser to avoid coupling high power. The 20 μW and 30 μW were coupled successfully by bending and slowly releasing the silica fiber, however, once the bending loss is removed (i.e. once the fiber is stretched) the material suddenly melts and evaporates due to high input power as shown in figure 3.13.

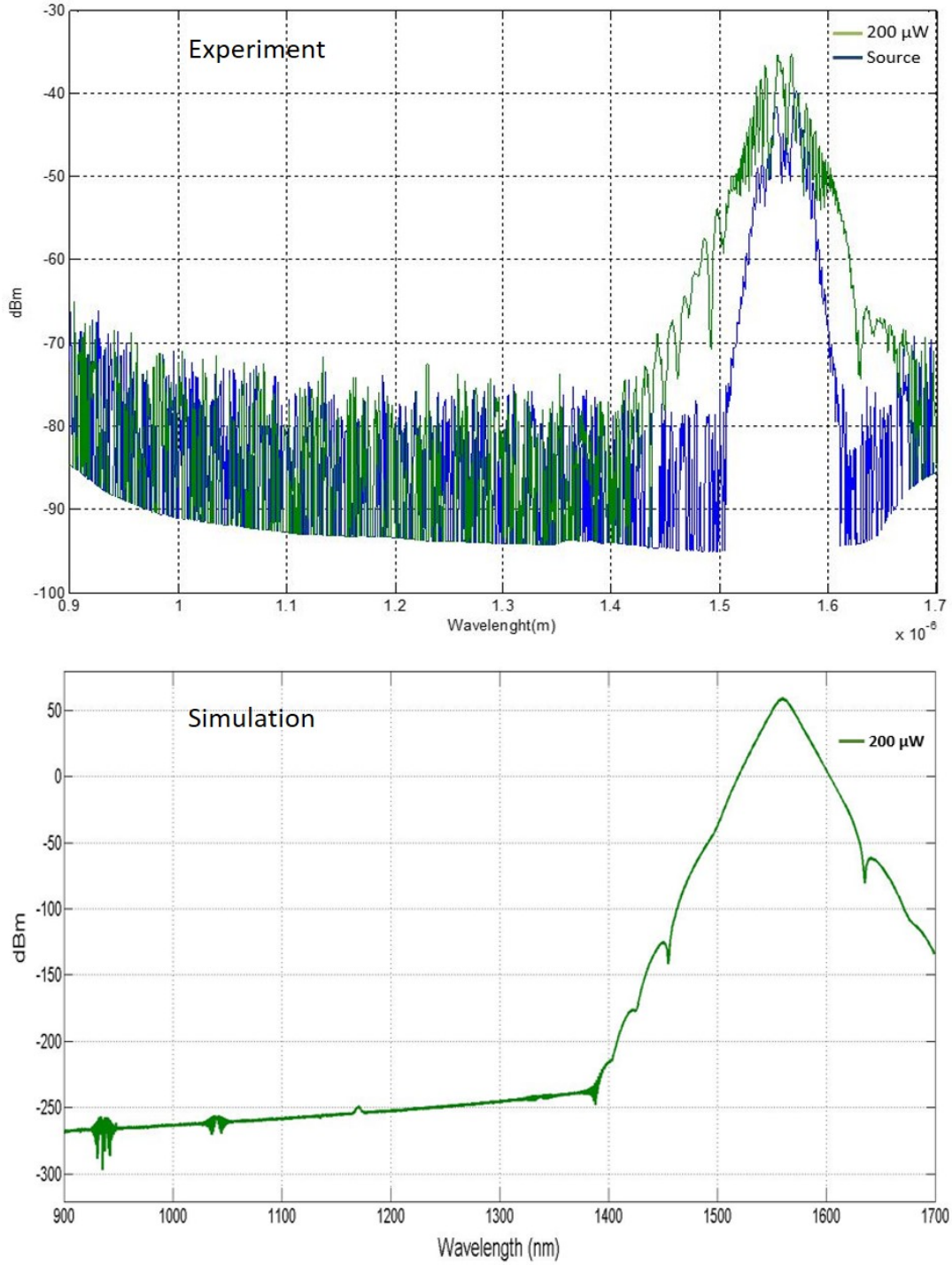

Figure 3.15: Experimental and numerical data showing output spectrum for supercontinuum generation in As_2S_3, where blue is the source pulse/incident pulse spectrum, green is the output spectrum at 200 μW.

Figure 3.15 represents both experimental and numerical output spectra for SCG with As_2S_3. Same simulation parameters used for As_2Se_3 were used here, except γ for As_2S_3 was calculated to be $\gamma = 2.32\ W^{-1}m^{-1}$. Again, a good agreement between experiment and simulation is reached, this indeed verifies the credibility of our experiment. Although as can be seen from the figure an average input power of 200 μW was able to be coupled into a tapered As_2S_3 fiber, the broadening extent in the output spectrum is somewhat similar to that of As_2Se_3. Apparently, this is a clear manifestation of the fact that optical nonlinearity in As_2Se_3 is an order of magnitude greater than that of As_2S_3 [56], though optical nonlinearity in As_2S_3 is still two orders of magnitude greater than that of silica. Furthermore, an important advantage of As_2S_3 over As_2Se_3 worth mentioning is the power handling capability of tapered As_2S_3. Whereas strong absorption in As_2Se_3 at high average input powers leads to sudden melting and evaporation of tapered As_2Se_3 which is an undesirable effect. Therefore by minimizing losses and ensuring that sufficient power is coupled into the tapered As_2S_3 fiber, a severe spectral broadening can be obtained.

Chapter 4

Multicore chalcogenide fibers for supercontinuum generation

Research on supercontinuum generation mainly focuses on three important challenges: Maximization of spectral broadening for several spectral regions, minimization of the input power threshold for supercontinuum generation, and maximization of a supercontinuum output power. The first challenge (i.e. maximization of the output spectrum) can be achieved by using a material with large transparent window at longer wavelengths such as chalcogenide glasses which shows great transparency in the infrared region. On the contrary, silica has strong vibrational absorption at these long wavelengths thereby limiting spectral broadening due to strong absorption. A recent study demonstrated a dramatic spectral broadening covering 1.4 μm - 13.3 μm molecular fingerprint region using ultra-high NA multimode chalcogenide step-index fibre which has an As_2Se_3 core and $Ge_{10}As_{23.4}Se_{66.6}$ cladding [57]. Another study showed infrared supercontinuum generation spanning more than one octave, using a picosecond laser at 1.55 μm [58]. For the second challenge tapering happened to be one of the most promising solution [59]. For instance, spectral broadening between 1.15 μm - 1.65 μm in tapered As_2Se_3 was obtained while pumping at a very low peak power of $P_p = 7.8W$ [60]. Also in the preceding chapter we demonstrated spectral broadening in As_2Se_3 with a peak power as low as $P_p = 2$ W.

The effort to tackle the third challenge was at first predominantly devoted to silica and doped silica photonic crystal fibers (PCF). For instance, a generation of 5 W average power and a SC covering 500 nm - 1800 nm was demonstrated with a single core silica PCF using picosecond pulses [61]. The main challenge associated with high power SCG in single core silica fibers are damages occurring at the pump facet or inside the fiber due to high pump intensity. Hence, high power SCG in multi-core silica PCF prove promising- an ouput power as high as 42.3 W and SC covering wavelength range from 720 nm to beyond 1.7 μm using a seven core silica PCF with picosecond pulses [62]. Furthermore, a new record of 112 W output power SC spanning at least 500 nm - 1700 nm was demonstrated using similar seven core silica PCF while pumping with picosecond pulses [63].

In general, spectral broadening beyond 2.4 μm in silica fibers is perhaps not feasible due to strong vibrational absorption at longer wavelengths as mentioned previously. Herein, we aim to tackle the outlined three fundamental challenges in supercontinuum generation with optical fibers using one single approach inspired by the seven core silica PCF. We fabricated a sub-micron multicore chalcogenide step index fiber rather than just seven core.

4.1 Fabrication

In this section we will briefly present a comprehensive fabrication details, for further details regarding fabrication and characterization of the fiber one can refer to [64].

4.1.1 Preform preparation

A preform is a macroscopic structure which represents the geometry of the to-be-drawn micro/nanofiber. Hence, preform preparation is a crucial aspect of fiber fabrication, any failure or error can lead to undesired consequences in the fiber drawing process which will directly affect the geometry of the drawn fiber.

Therefore a diligent preform preparation is paramount for drawing of excellent fibers.

Preform preparation comprises of three parts; a core which guides light through, a cladding which provides refractive index difference thereby enhancing light confinement within the core, and a polymer jacket which serves as a protective jacket, hence, provides mechanical support as well as flexibility to the drawn fiber (for more fundamental insight [65]). The core and cladding comprises of As_2Se_3 and $Ge_{10}As_{23.4}Se_{66.6}$ respectively, and were prepared using melt quenching and rotational casting technique respectively. Raw materials were batched into a quartz ampoule sealed and vacuumed in order to maintain purity. An As_2Se_3 rod of 8 mm diameter was extracted after quenching in water by simply breaking the quartz tube. And the rotationally casted quartz tube (i.e. the cladding) was obtained by quenching in air, it has an inner diameter similar to the rod (i.e. core) diameter and an outer diameter of 10.3 mm, the fabricated rod (core) perfectly fits into the tube (cladding). At this point, it is important to mention that a chalcogenide glass of lower index was chosen as the cladding due to the fact that pumping polymer embedded chalcogenide leads to high absorption in the polymer in infrared region [66]. Therefore, to effectively explore our proposed method, chalcogenides are more suitable for cladding material due to their low loss in the infrared region. Moreover, a combination of such high index materials as core and cladding yields high numerical aperture thereby enhancing light coupling.

The polymer jacket was fabricated from Polyethylenimine (PEI) via thin polymer film rolling and consolidation. And a hollow PEI polymer rod with an inner diameter approximately equal to that of the cladding outer diameter and a total diameter of 25 mm -28 mm was fabricated.

After successful fabrication of all the three important components namely core, cladding and polymer jacket, the preform was obtained by combination/fusion of the three components, the resultant preform as well as the schematic representation of its design can be seen in figure 4.1 a) and b). where c) corresponds to the numerical aperture/refractive index as a function of wavelength.

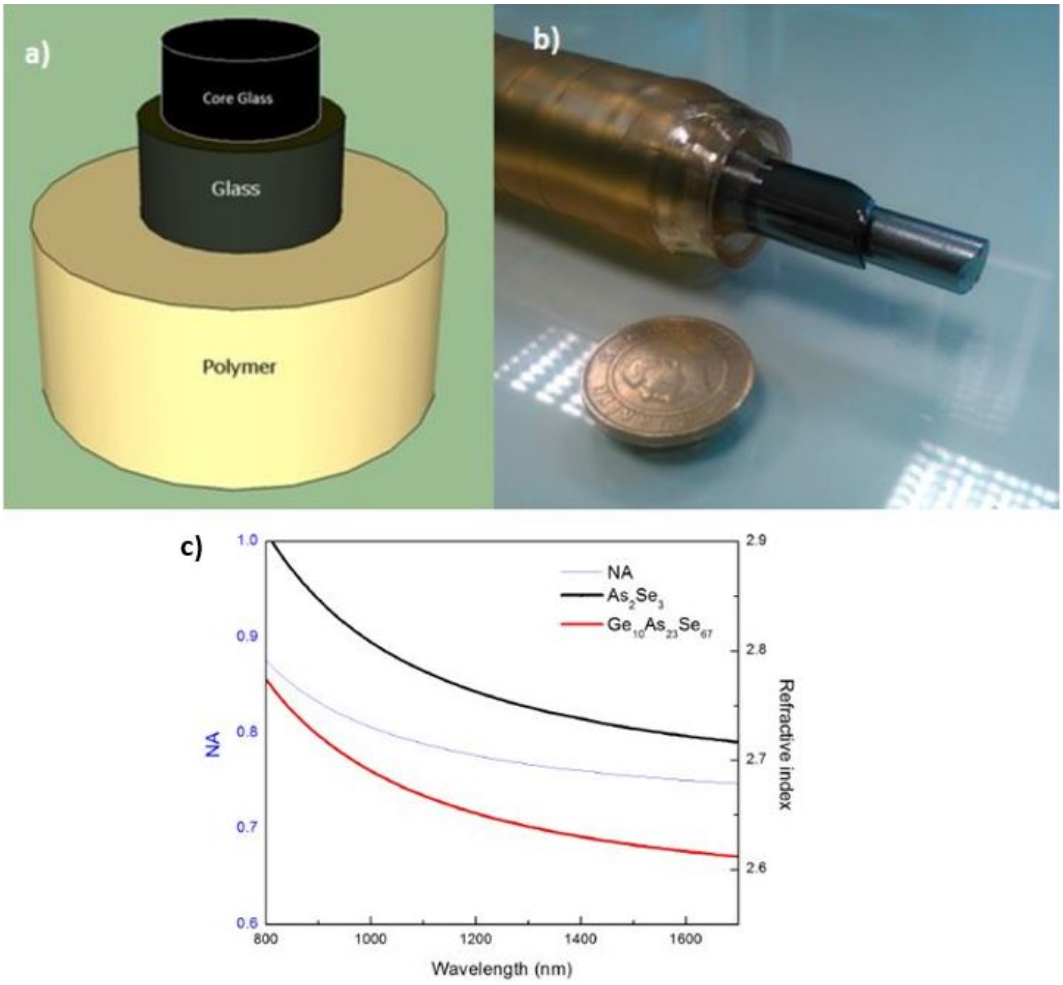

Figure 4.1: a) Schematic representation of the preform design b)prepared preform, c) shows refractive indices as well as numerical apertures of the chalcogenide materials as a function of wavelength [64].

4.1.2 Fabrication of multicore fiber

In general, optical fibers are fabricated by thermally drawing of a macroscopic preform. Here the fibers were drawn using an iterative size reduction technique. Yaman et al. [67] introduced a new technique known as iterative size-reduction (ISR) method, which can fabricate an indefinitely long nanowire arrays in a flexible polymer fiber matrix from a multimaterial macroscopic rod. A fiber drawing tower for the ISR method can be seen in Figure 4.2.

The multicore fibers were fabricated in three steps using the ISR method. For the first step drawing, the prepared macroscopic preform with diameter 26.5 mm was suspended appropriately in the fiber drawing tower, and the fiber diameter was fixed to 1.6 mm which corresponds to a reduction factor of 16.56, this implies that the drawn fiber will have a core diameter of $\sim 480\ \mu m$ and that of cladding $\sim 600\ \mu m$. Figure 4.3 shows the dark field and bright images of the 1^{st} step fiber.

Figure 4.2: Fiber tower for the drawing process and the corresponding components of the fiber tower [67]

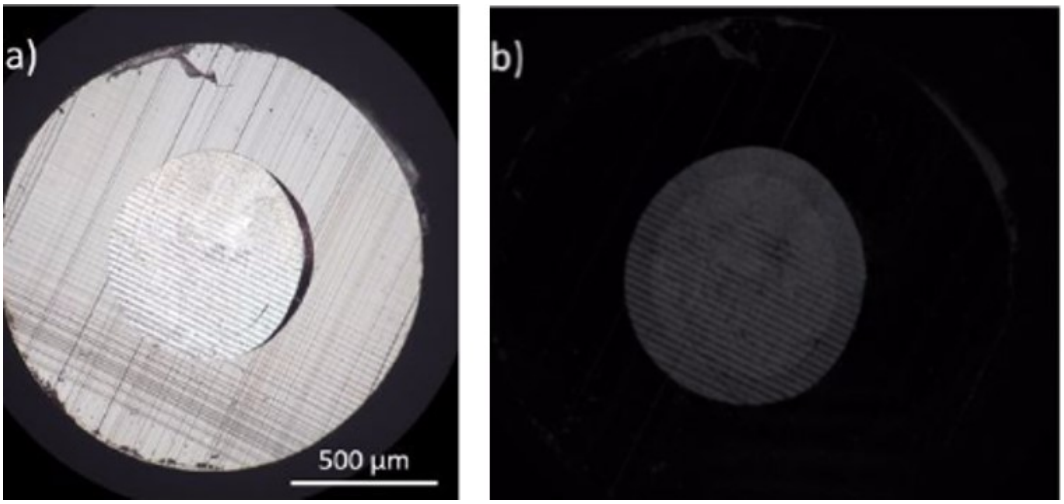

Figure 4.3: a) bright field, b) dark field. The boundaries between cladding and polymer are obvious in the bright field image but it is not possible to distinguish the core. However, the boundary between core and cladding becomes distinguishable in the dark field image [64].

The second step drawing involves a process known as stack and draw process. A PEI tube was fabricated with an inner and outer diameter of 8 mm and 26 mm respectively, the first step drawn fiber was cut into pieces of 10 cm long each. And then seven pieces of the first step fiber were stack in a hexagonal geometry into the PEI tube and drawn using similar procedure as in the first step. Where the reduction factor was calculated to be 17.33 which corresponds to a total fiber core/cladding diameter of 35 μm. Figure 4.4 a) shows a micrograph of the second step fiber with the seven cores in a hexagonal geometry.

For the third step drawing, fibers drawn in second step are cut into 15 cm long pieces, similarly, 34 of them were stacked into a PEI rod of ID and OD 8 mm and 26 mm respectively and drawn. The reduction factor here was found to be 26, thereby reducing the total diameter of ChGs to 135 μm with a core diameter of ~ 1 μm. Micrograph showing multiple array of the seven core fibers in the third step fiber can be seen in figure 5.5 b).

The dispersion parameter of the drawn fiber was calculated using Lumerical Mode solution, Figure 4.5 shows the dispersion parameter of the fiber design with respect to core diameter. Where a zero dispersion was observed at 1.1 μm,

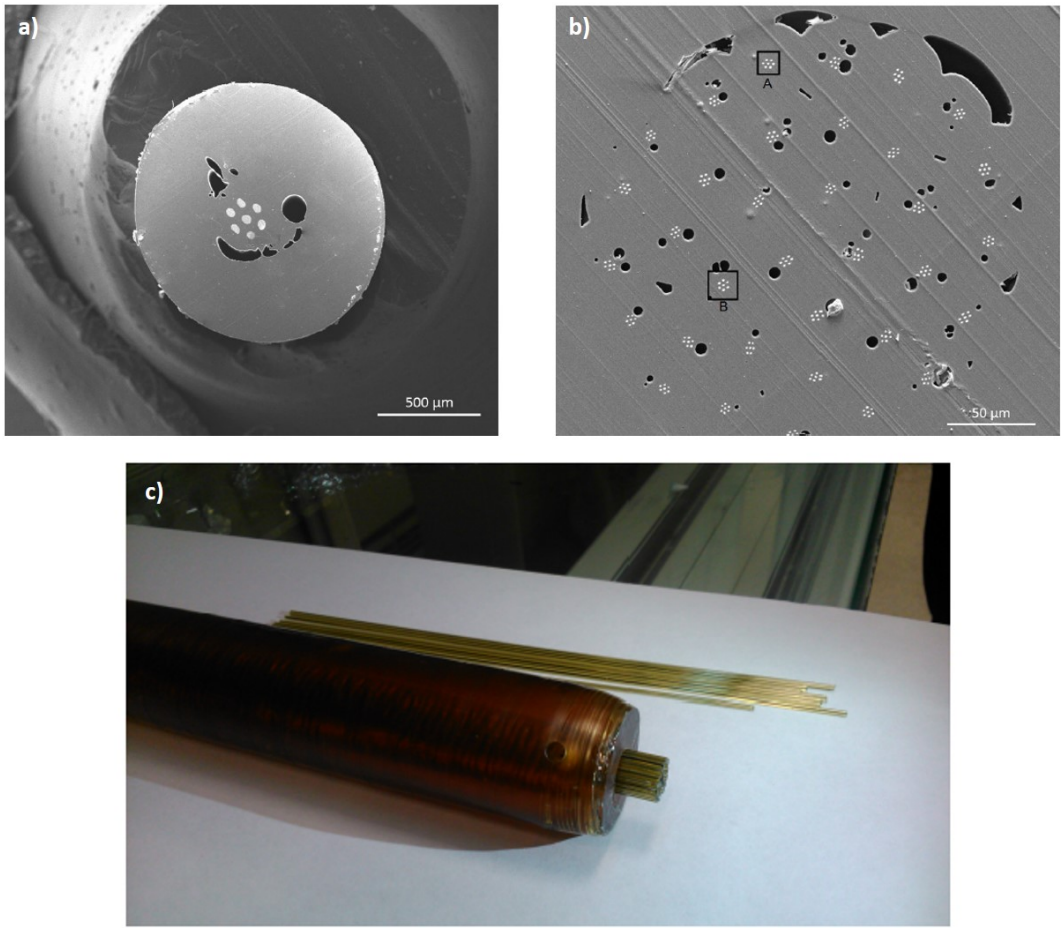

Figure 4.4: a) and b) are micrographs of the second and third step fibers, while c) depicts stacking of fibers into a polymer rod [64].

remember, for the third step fiber the core diameter was found to be 0.95 μm which falls in the anomalous dispersion regime just close to the ZDW, and has a dispersion parameter of approximately 100 ps/nm-km, which is a relatively small value compared to the material dispersion and this value of dispersion corresponds to a group velocity dispersion of $\beta_2 = -0.128\ ps^2/m$. Note that, pumping extremely close to the ZDW leads to an effective spectral broadening.

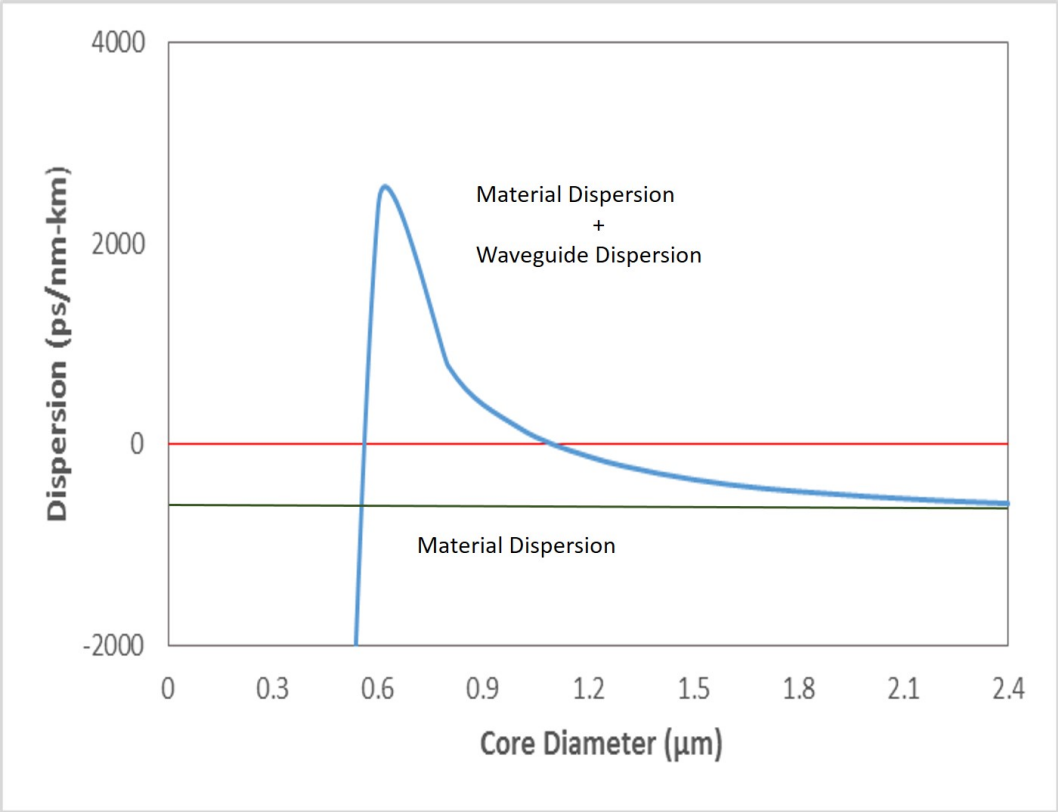

Figure 4.5: Calculated dispersion parameters for core/cladding fiber design with respect to core diameter at pump wavelength of $1.55\mu m$. The green line represents material dispersion of bulk core material (As_2Se_3).

4.2 Experimental demonstration of SCG

In this section, experimental demonstration of SCG in the as-drawn fibers as well as some of the the encountered challenges will be discussed. Also proposed unique solutions to these challenges will be demonstrated and discussed.

Before light is coupled into a waveguide, an optical quality polishing is extremely vital for proper coupling of light into a waveguide. The polishing device used to polish the third step fiber was a Bare Fiber Polisher (Krelltech,Trig), which is shown in 4.6 a). However, the third step fiber could not fit into the device holder(i.e. 2 in 4.6 a)), hence, a plastic holder which was designed to hold the fiber firmly was printed usig 3D printer as shown in 4.6 b). $\sim$ 1 cm of the third step fiber was suspended vertically in a plastic container and held firmly to

avoid any bending, and then the container was filled with an an epoxy (Technoviz 7100) containing a ratio of 1:15 of hardener to resin. A UV curing of about 15 mins was carried out in order to initiate polymerization, and then waited for 24 hours after UV curing of the epoxy for proper hardening. A hard third step fiber embedded in epoxy (TSFEE) was obtained by simply getting rid of the plastic container. Due to flat facets on either sides of the TSFEE, precise polishing is extremely tedious, therefore pyramidal shapes were made on either sides of the facet using MICROTOME (LEICA EM UC6) as shown in Figure 4.6 c). This provide precision during polishing. The 3D printed holder serves as an interconnect between the micro-machined TSFEE and the polisher. Consequently, an optical quality polishing of the TSFEE was obtained as can be seen in 4.6 d).

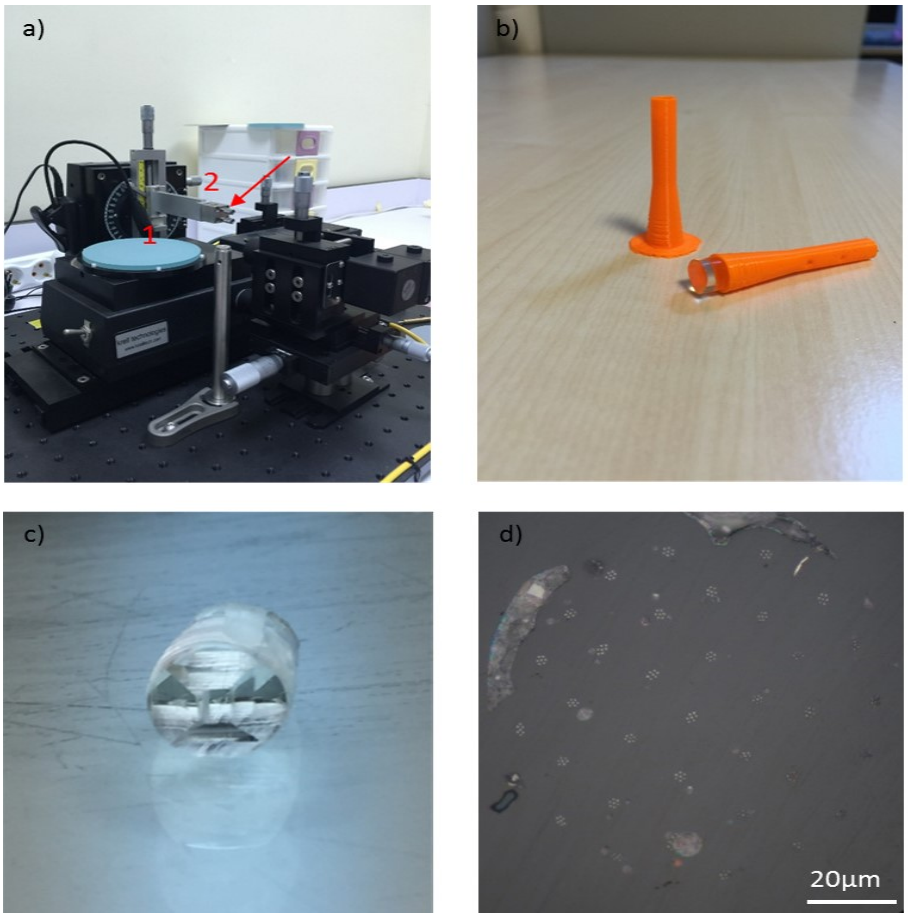

Figure 4.6: a) Bare Fiber Polisher (Krelltech,Trig where 1 is a motorized rotating sand paper and 2 is a holder to which the fiber is attached, b) 3D printed holder, c) micromachined TSFEE and d) polished TSFEE.

Similar setup used in Figure 3.10 (i.e. all-fiber butt coupling rather than free space coupling) was used here, just that the tapered fiber in 3.10 was replaced by the polished multicore fiber as shown in 4.7. Although using a thermal camera located just above the sample, weak light coupling was observed as can be seen in 4.8 b), no any broadening in the output spectrum was observed (as seen 4.8 a)). It was suggested that sufficient amount of power was not coupled into the fiber cores due to the random distribution of the multicore array.

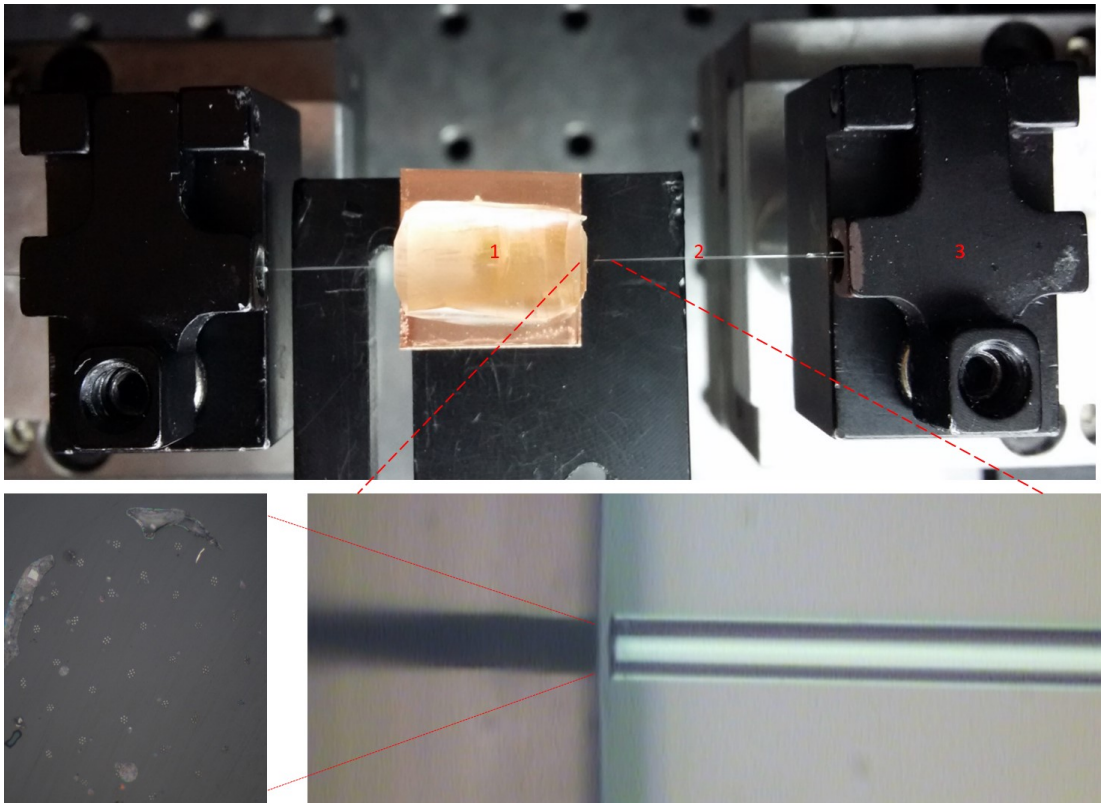

Figure 4.7: Setup for Supercontinuum generation, 1 is the sample, 2 is the tapered silica fiber and 3 is the motorized stage/clamp.

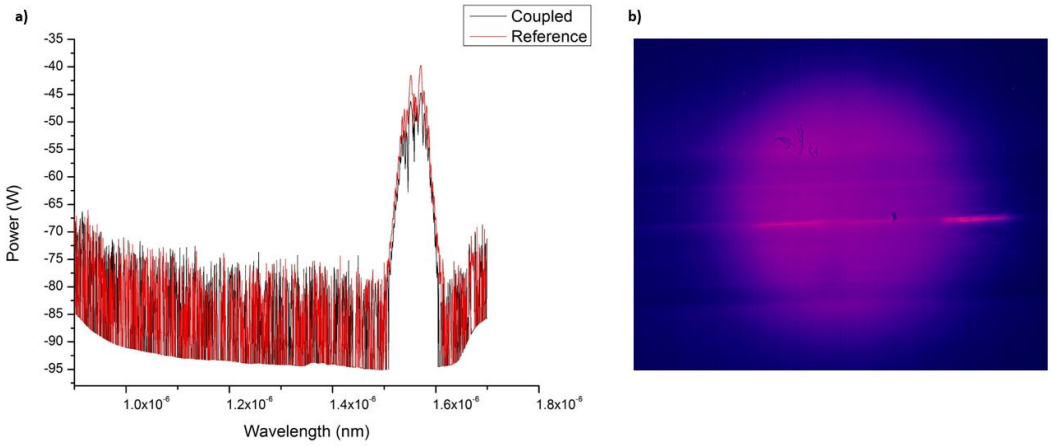

Figure 4.8: Output spectrum a), coupling under a thermal camera b).

4.2.1 Collapsed bundle

In order to have sufficient light coupling into some cores of the multicore fiber array, the PEI polymer jacket was etched using dichloromethane (DCM). The etching transforms the multicore array into a densely packed bundle of multicore chalcogenide step index fibers (which is referred to as collapsed bundle). This will perhaps ensure sufficient light coupling into certain cores within the densely packed cores. Figure 4.9 a) and b) shows SEM images of the collapsed bundle lateral and cross sectional views respectively. Before etching, certain region at both top and bottom of the fiber were wrapped with a Teflon tape in order to prevent etching, since Teflon resists DCM. These unetched parts will provide mechanical support to the whole fiber during and after etching. The fiber was then placed in a container and held firmly. Little holes were made at both top and bottom of the container in order to stimulate flow when DCM is injected for etching (4.9 c)). After successful etching, the bottom holes were closed and epoxy (just like described in the previous subsection) was filled from the top. This embeds the densely packed fibers, thereby providing a mechanical support and preventing any physical damage. After proper hardening, the collapsed bundle was micro-machined and polished similar to that discussed in Figure 5.8. Figure 4.9 d) shows an optical image of a well polished and densely packed bundle.

Using same setup like that in Figure 5.9, light was coupled to the collapsed bundle and observed by a thermal camera. Significant amount of light was coupled, however, at a certain region along the fiber a tremendous scattering point was observed (Figure 4.9 e)), at which further coupling seriously diminished. Upon further investigation under a microscope, it was noticed that the assumed scattering point was as a result of a micro kink along the fiber as shown in 4.9 f). The experiment was repeated several times using various approaches, however, micro kinks kept reoccurring.

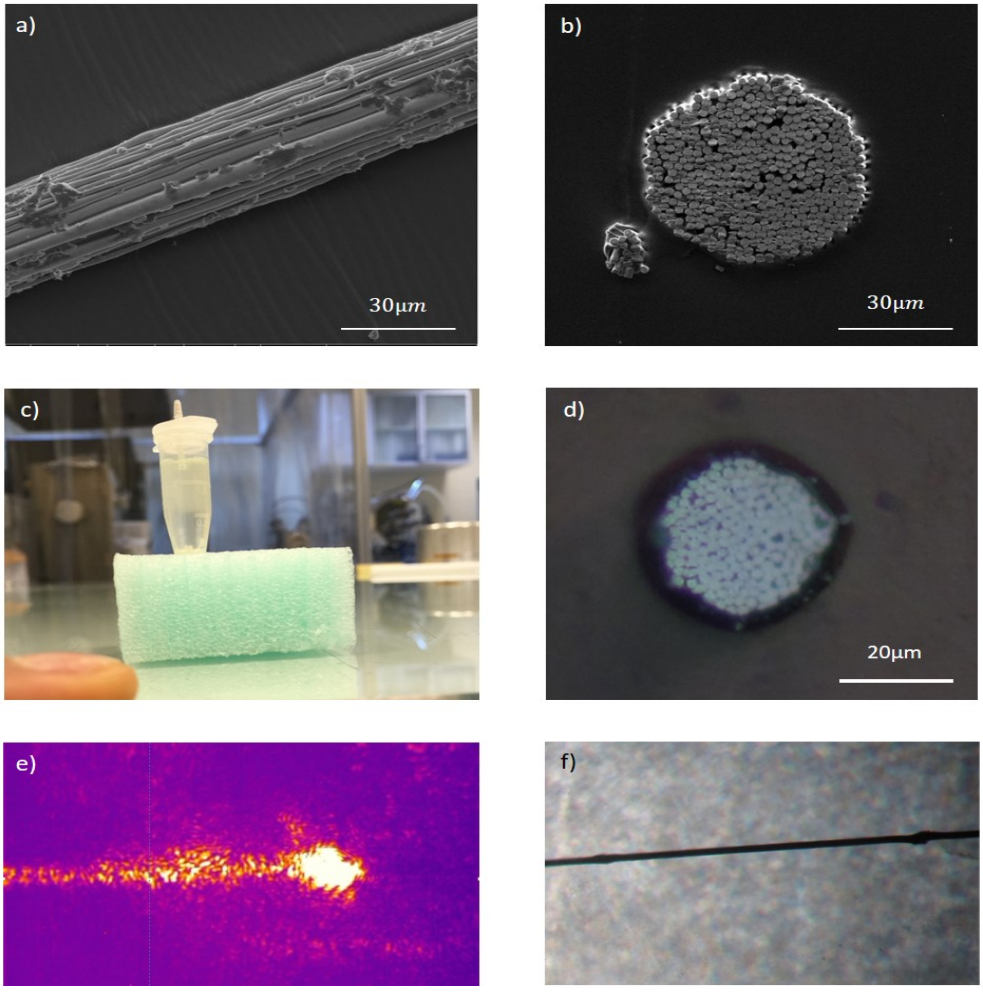

Figure 4.9: a) and b) are collapsed bundle SEM images for lateral and cross sectional views respectively, c) represents etching and epoxy, d) shows the polished collapsed bundle, e) thermal camera image of the scattering point and f) is the micro kink.

In order to tackle the reoccurring microkink along the fiber, a new technique for collapsed bundle was developed. Figure 4.10 shows a schematic representation of the new technique for the collapsed bundle. At first the multicore fiber was dip coated with Polyvinylidene fluoride (PVDF) dissolved in Dimethylformamide (DMF), the PVDF + DMF coated fiber was then put into an oven at 100 C for an hour to facilitate homogeneity. PVDF was then removed from the region to be etched (Figure 1.10(2)). Figure 4.11 a) clearly depicts the PVDF coated and uncoated regions. The PVDF removed region was etched in DCM without any defect meanwhile the PVDF coated region remains unetched, as can be seen in Figure 4.10(3) and Figure 14.11 b). The fiber was then polished on either facets after proper epoxy and micromachining (Figure 4.10 (4,5) and Figure 4.11 c)).

Some important advantages of this technique worth mentioning include the fact that the etched region converges (i.e. the cores become closely packed) which ensures effective coupling. Also the PVDF coated region (i.e. the unetched region) provides flexibility along the fiber ensuring no physical defect along the fiber (Figure 4.10(5) and 4.11 c)).

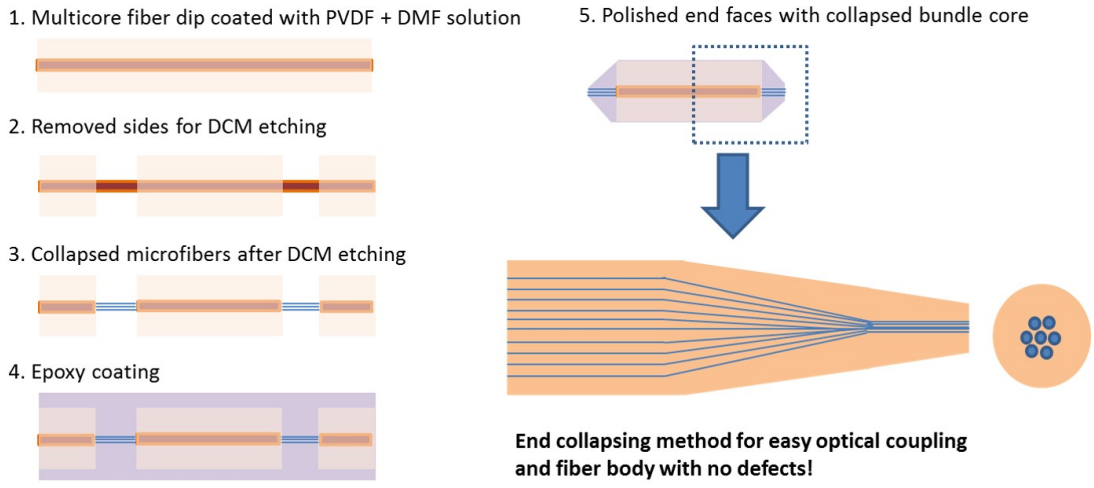

Figure 4.10: Schematic representation of a new technique for collapsed bundle.

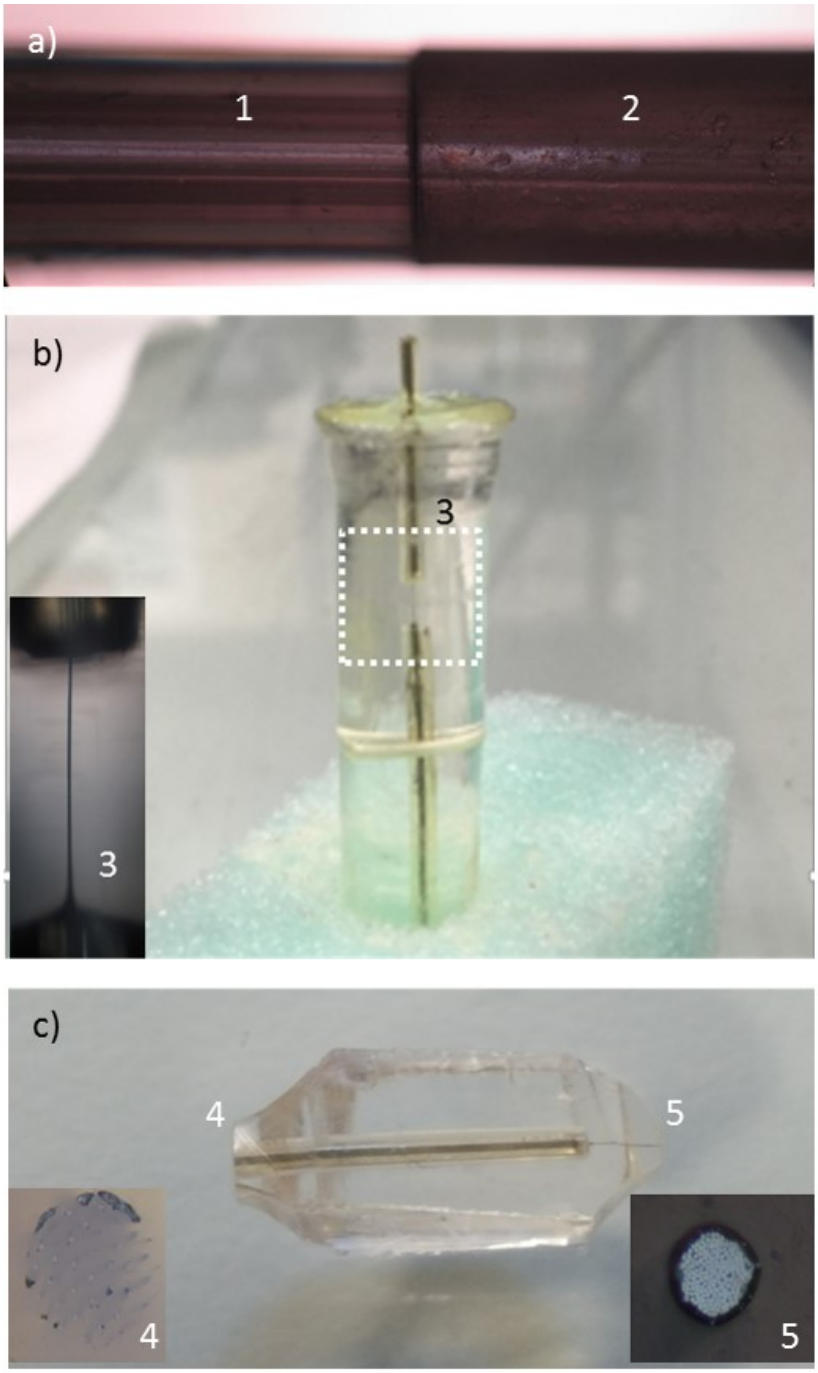

Figure 4.11: a) shows the pvdf coated region 2 and uncoated region of the fiber 1 which was mechanically removed. b) clearly shows the pvdf uncoated was successfully etched with no defect, and c) shows the whole fiber aftre micromachining and polishing.

4.3 Discussion

The technique is quite promising and unique, light was coupled into the fiber without any scattering point along it, however, no spectral broadening was observed. It was suggested that this might be due to insufficient focusing/coupling of light into the bundle cores via butt coupling. Hence ensuring precise and effective focusing/coupling may yield severe spectral broadening as well as high output power.

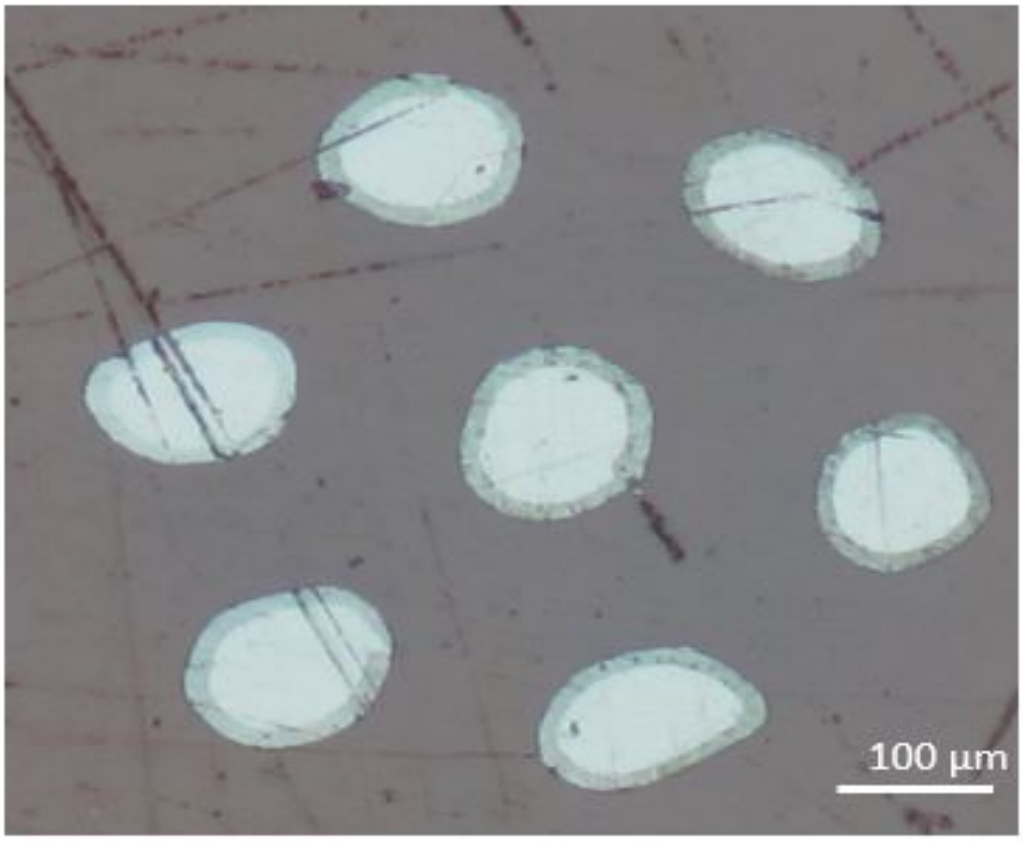

Figure 4.12: Optical microscopic image of the multicore fiber cross section.

It was also suggested that the irregular shape of the cores (as shown in Figure 4.12) undermines coupling into the fiber which is even more pronounce when butt coupling. Also such irregular core shapes can undermine light propagation inside the fiber. Furthermore, changing core shape toward a non-circular profile can also undermine spectral broadening [68].

Nevertheless, we numerically demonstrate the great potential of this technique for severe spectral broadening at extremely low peak powers. Using a calculated effective area of $A_{eff} = 0.69\ \mu m$, pulse duration of $\tau_0 = 150$ fs, at $\lambda_0 = 1550$ nm, β_2 = -0.128 $\frac{ps^2}{m}$, $\gamma = 23.2\ W^{-1}m^{-1}$ and a fiber length of $l = 15cm$, we numerically model supercontinuum generation in a single core of the as drawn multicore chalcogenide step-index fiber at extremely low peak powers (Figure 4.13).

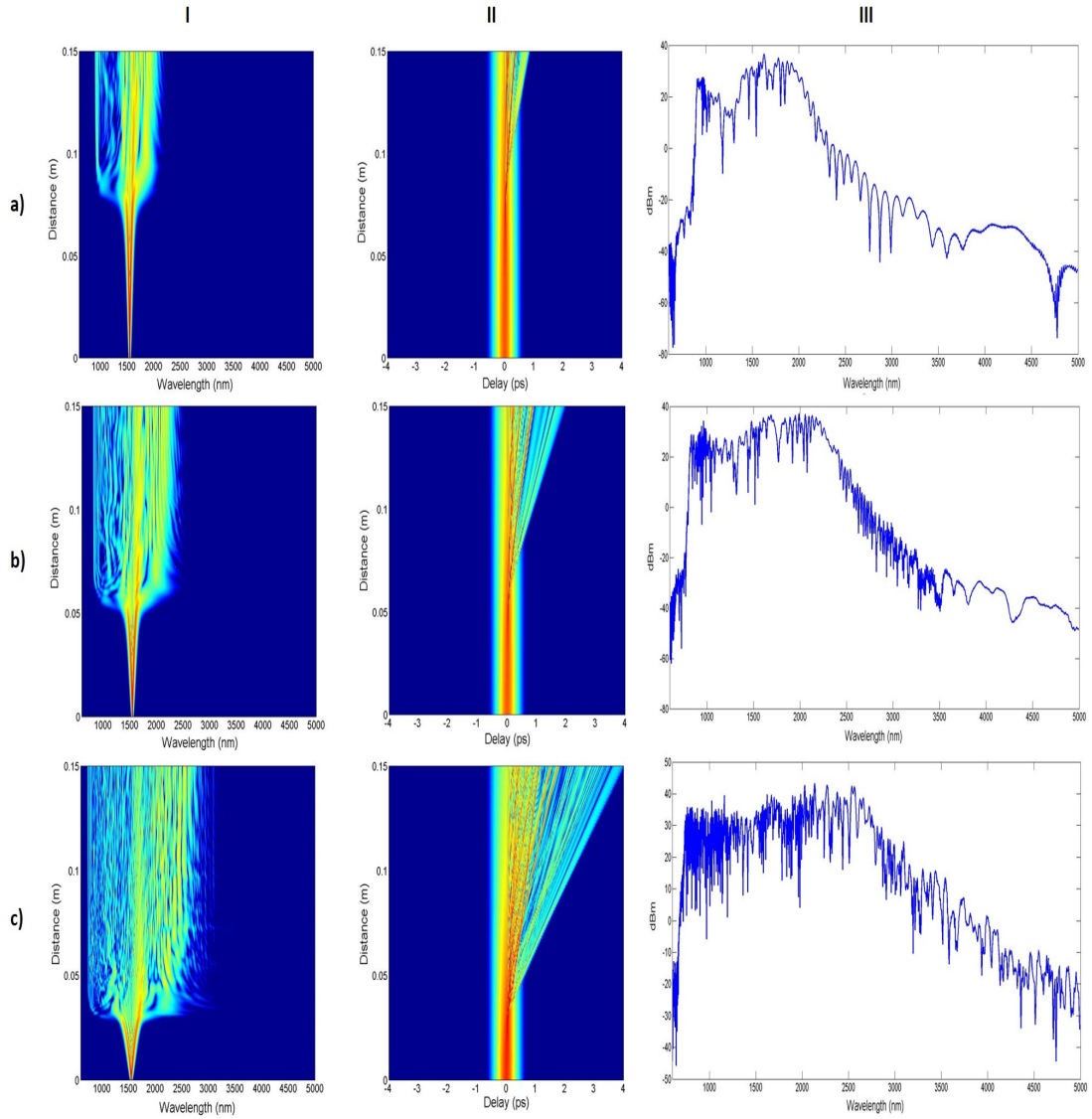

Figure 4.13: I, II, and III are colorscale and line plot representations for spectral and temporal evolution of SC inside highly nonlinear 15 cm length of single fiber with As_2Se_3 core for different peak powers a) 5 W, b) 10 W, and d) 30 W.

For pump at peak powers 5 W, 10 W, 30 W were calculated to have a soliton order N of 4, 6, and 11 respectively which correspond to higher order solitons. Considering the fact that we are pumping in the anomalous GVD regime very close to the zero dispersion, these higher order soliton will experience some perturbation (due to higher order order dispersions and Raman effects) which leads to break up of higher order solitons into fundamental solitons (also known as soliton fission) and generating dispersive waves. Generated dispersive waves leads to spectral broadening in the short wavelength regime whilst in the long wavelength regime soliton fission and Raman self frequency shift are responsible.

When pumping at 5 W peak power, after a propagation distance of $\sim 8\ cm$ we begin to observe severe spectral broadening, also soliton fission and dispersive wave generation become more pronounced (Figure 4.13 a) I and II), and (Figure 4.13 a) III) shows the corresponding line plot of the spectral evolution. However, when pumping at 10 W peak power, soliton fission as well as dispersive generation happened after shorter propagation distance ((Figure 4.13 b) I and II)) compared to that pumping at 5 W. And this is because the Raman effect is power dependent, therefore, more power means more perturbation of higher order solitons due to Raman effect, hence, faster spectral evolution. Figure (4.13 b) III) shows the corresponding line plot of the spectral evolution. And at 30 W peak power, indeed soliton fission as well as dispersive generation occurs at much shorter propagation distance (Figure 4.13 c) I and II) and the corresponding line plot for the spectral evolution is shown in (Figure 4.13 c) III). The extent of spectral broadening indeed scales peak power.

Chapter 5

Conclusion and future works

To address the fundamental challenges associated with supercontinuum generation with optical fibers, we proposed two unique fabrication techniques namely Direct tapering and Multicore fibers.

Nanowires/nanofibers were fabricated directly from bulk chalcogenide glasses, and we referred to the technique as 'Direct tapering'. Furthermore, spectral broadening with extremely low input power was demonstrated via direct tapering of bulk As_2Se_3 and As_2S_3. However, severe spectral broadening was not observed, because of tremendous amount of losses (such as Fresnel, absorption and butt to butt coupling losses) in the input power. Third harmonic generation (THG) was also observed. THG kept reoccurring even when pumping at various pump powers in both As_2Se_3 and As_2S_3. This leads to absorption losses in the input power, where at elevated input powers As_2Se_3 evaporates. Although even in the presence of THG, As_2S_3 proved a better power handling capability, however it still undermines the input power thereby hindering supercontinuum generation.

As a future plan, we will try to minimize butt to butt coupling losses by minimizing the number of butt to butt couplers as well as inter connects in the optical set up. We may also try free space coupling in order to provide sufficient power for supercontinuum generation. We will also engineer some parts of tapering

in order to mitigate THG especially in As_2Se_3, which proves vulnerable due to absorption of 520 nm light generated via THG. Also, longer wavelength sources (Mid-IR) can be more suitable for our technique [69–71].

Multicore step index chalcogenide fibers with $\sim 1\mu m$ diameter and engineered ZDW around 1550nm were successfully fabricated using a new method. Numerical results have proven the fabricated fibers to be promising, where severe spectral broadening with extremely low input powers were shown using split-step Fourier method. However, sufficient light coupling into the cores of the multicore fiber has proven difficult, due to the disperse nature of the cores within the fiber array. Therefore, in order to mitigate this challenge a new technique which is termed 'Collapsed bundle' was developed. The PEI polymer which embeds the chalcogenide fibers was etched using DCM, which gave rise to a densely packed step index chalcogenide fiber bundle, which will perhaps facilitate coupling. Again sufficient coupling was not achieved. Upon further investigation, the fibers were found to have an arbitrary shape. It was suggested that such irregular core shapes undermines coupling particularly when butt coupling.

It is apparent that due to the irregular shape of the fiber, butt coupling of such fibers is extremely tedious. Therefore, experiment will be repeated using free space coupling, in order to sufficiently couple light into the multicore array, and supercontinuum generation will be observed. A severe spectral broadening can be observed once sufficient amount of light is successfully coupled into the multicore array.

Bibliography

[1] R. Alfano and S. Shapiro, "Emission in the region 4000 to 7000 å via four-photon coupling in glass," *Physical Review Letters*, vol. 24, no. 11, p. 584, 1970.

[2] R. R. Alfano *et al.*, "The supercontinuum laser source," 1989.

[3] A. B. Seddon, "A prospective for new mid-infrared medical endoscopy using chalcogenide glasses," *International Journal of Applied Glass Science*, vol. 2, no. 3, pp. 177–191, 2011.

[4] M. G. Allen, "Diode laser absorption sensors for gas-dynamic and combustion flows," *Measurement Science and Technology*, vol. 9, no. 4, p. 545, 1998.

[5] B. J. Eggleton, B. Luther-Davies, and K. Richardson, "Chalcogenide photonics," *Nature photonics*, vol. 5, no. 3, pp. 141–148, 2011.

[6] R. Wilson and H. Tapp, "Mid-infrared spectroscopy for food analysis: recent new applications and relevant developments in sample presentation methods," *TrAC Trends in Analytical Chemistry*, vol. 18, no. 2, pp. 85–93, 1999.

[7] Y. Sun, C. F. Booker, S. Kumari, R. N. Day, M. Davidson, and A. Periasamy, "Characterization of an orange acceptor fluorescent protein for sensitized spectral fluorescence resonance energy transfer microscopy using a white-light laser," *Journal of biomedical optics*, vol. 14, no. 5, pp. 054009–054009, 2009.

[8] A. E. Siegman, "Lasers university science books," *Mill Valley, CA*, vol. 37, p. 208, 1986.

[9] P. Vasil'ev, "Ultrafast laser diodes: Fundamentals and applications," *Artech House, London*, 1995.

[10] S. T. Cundiff, J. Ye, and J. L. Hall, "Optical frequency synthesis based on mode-locked lasers," *Review of Scientific Instruments*, vol. 72, no. 10, pp. 3749–3771, 2001.

[11] P. Russell, "Photonic crystal fibers," *science*, vol. 299, no. 5605, pp. 358–362, 2003.

[12] E. C. Mägi, L. Fu, H. C. Nguyen, M. Lamont, D. Yeom, and B. Eggleton, "Enhanced kerr nonlinearity in sub-wavelength diameter as2se3 chalcogenide fiber tapers," *Optics Express*, vol. 15, no. 16, pp. 10324–10329, 2007.

[13] D.-I. Yeom, E. C. Mägi, M. R. Lamont, M. A. Roelens, L. Fu, and B. J. Eggleton, "Low-threshold supercontinuum generation in highly nonlinear chalcogenide nanowires," *Optics letters*, vol. 33, no. 7, pp. 660–662, 2008.

[14] R. Stolen and A. Ashkin, "Optical kerr effect in glass waveguide," *Applied Physics Letters*, vol. 22, no. 6, pp. 294–296, 1973.

[15] K. Hill, D. Johnson, B. Kawasaki, and R. MacDonald, "cw three-wave mixing in single-mode optical fibers," *Journal of Applied Physics*, vol. 49, no. 10, pp. 5098–5106, 1978.

[16] R. Stolen and C. Lin, "Self-phase-modulation in silica optical fibers," *Physical Review A*, vol. 17, no. 4, p. 1448, 1978.

[17] J. Sanghera and D. Gibson, "Optical properties of chalcogenide glasses and fibers-5," 2014.

[18] K. R. J.D. Musgraves, S. Danto, "Thermal properties of chalcogenide glasses-4," 2014.

[19] S. P. Singh and N. Singh, "Nonlinear effects in optical fibers: Origin, management and applications," *Progress In Electromagnetics Research*, vol. 73, pp. 249–275, 2007.

[20] G. Agrawal, *Applications of nonlinear fiber optics*. Academic press, 2001.

[21] P. Diament, *Wave transmission and fiber optics*. Macmillan, 1990.

[22] A. M. Weiner, "Ece 616 lecture 20: Propagation equation for nonlinear refractive index media," 2011.

[23] J.-K. Kim, "Investigation of high-nonlinearity glass fibers for potential applications in ultrafast nonlinear fiber devices," 2005.

[24] C. Garrett and D. McCumber, "Propagation of a gaussian light pulse through an anomalous dispersion medium," *Physical Review A*, vol. 1, no. 2, p. 305, 1970.

[25] C. Lin, L. Cohen, and H. Kogelnik, "Optical-pulse equalization of low-dispersion transmission in single-mode fibers in the 1.3–1.7-μm spectral region," *Optics letters*, vol. 5, no. 11, pp. 476–478, 1980.

[26] G. P. Agrawal and M. Potasek, "Effect of frequency chirping on the performance of optical communication systems," *Optics letters*, vol. 11, no. 5, pp. 318–320, 1986.

[27] D. Anderson, P. Anderson, and M. Lisak, "Nonlinearly enhanced chirp pulse compression in single-mode fibers," *Optics letters*, vol. 10, no. 3, pp. 134–136, 1985.

[28] D. Marcuse, "Pulse distortion in single-mode fibers," *Applied Optics*, vol. 19, no. 10, pp. 1653–1660, 1980.

[29] G. P. Agrawal, "Chapter 3 group-velocity dispersion," in *Nonlinear Fiber Optics(Fourth Edition)*, vol. 8794, pp. 51–78, 2006.

[30] S. P. Singh and N. Singh, "Nonlinear effects in optical fibers: Origin, management and applications," *Progress In Electromagnetics Research*, vol. 73, pp. 249–275, 2007.

[31] F. Shimizu, "Frequency broadening in liquids by a short light pulse," *Physical Review Letters*, vol. 19, no. 19, p. 1097, 1967.

[32] T. Gustafson, J. Taran, H. Haus, J. Lifsitz, and P. Kelley, "Self-modulation, self-steepening, and spectral development of light in small-scale trapped filaments," *Physical Review*, vol. 177, no. 1, p. 306, 1969.

[33] R. Cubeddu, R. Polloni, C. Sacchi, and O. Svelto, "Self-phase modulation and" rocking" of molecules in trapped filaments of light with picosecond pulses," *Physical Review A*, vol. 2, no. 5, p. 1955, 1970.

[34] R. Alfano and S. Shapiro, "Direct distortion of electronic clouds of rare-gas atoms in intense electric fields," *Physical Review Letters*, vol. 24, no. 22, p. 1217, 1970.

[35] G. P. Agrawal, "Chapter 4 self-phase modulation," in *Nonlinear Fiber Optics(Fourth Edition)*, vol. 8794, pp. 79–119, 2006.

[36] R. A. Fisher and W. K. Bischel, "Numerical studies of the interplay between self-phase modulation and dispersion for intense plane-wave laser pulses," *Journal of Applied Physics*, vol. 46, no. 11, pp. 4921–4934, 1975.

[37] G. P. Agrawal, "Chapter 5 optical solitons," in *Nonlinear Fiber Optics(Fourth Edition)*, vol. 8794, p. 129191, 2006.

[38] A. Husakou and J. Herrmann, "Supercontinuum generation of higher-order solitons by fission in photonic crystal fibers," *Physical Review Letters*, vol. 87, no. 20, p. 203901, 2001.

[39] N. Kikuchi, K. Sekine, and S. Sasaki, "Analysis of cross-phase modulation (xpm) effect on wdm transmission performance," *Electronics letters*, vol. 33,

no. 8, pp. 653–654, 1997.

[40] G. P. Agrawal, "Chapter 10 four-wave mixing," in *Nonlinear Fiber Optics(Fourth Edition)*, vol. 8794, p. 368423, 2006.

[41] K. KRISHNAN, "A new class of spectra due to secondary radiation part i," *Indian J. Phys*, vol. 2, pp. 399–419, 1928.

[42] R. W. Boyd, S. G. Lukishova, and Y. Shen, *Self-focusing: Past and Present: Fundamentals and Prospects*, vol. 114. Springer Science & Business Media, 2008.

[43] G. P. Agrawal, "Chapter 8 stimulated raman scattering," in *Nonlinear Fiber Optics(Fourth Edition)*, vol. 8794, p. 274328, 2006.

[44] R. G. Smith, "Optical power handling capacity of low loss optical fibers as determined by stimulated raman and brillouin scattering," *Applied Optics*, vol. 11, no. 11, pp. 2489–2494, 1972.

[45] G. P. Agrawal, "Chapter 10 stimulated brillouin scattering," in *Nonlinear Fiber Optics(Fourth Edition)*, vol. 8794, p. 329367, 2006.

[46] J. M. Dudley and J. R. Taylor, *Supercontinuum generation in optical fibers*. Cambridge University Press, 2010.

[47] G. P. Agrawal, "Chapter 10 novel nonlinear phenomena," in *Nonlinear Fiber Optics(Fourth Edition)*, vol. 8794, p. 498501, 2006.

[48] B. Washburn, "Chapter iv - numerical solutions to the nonlinear schrdinger equation," in *Doctoral Thesis*, p. 134 157, 2005.

[49] T. A. Birks and Y. W. Li, "The shape of fiber tapers," *Journal of Lightwave Technology*, vol. 10, no. 4, pp. 432–438, 1992.

[50] D. Schaafsma, J. Moon, J. Sanghera, and I. Aggarwal, "Fused taper infrared optical fiber couplers in chalcogenide glass," *Journal of lightwave technology*,

vol. 15, no. 12, pp. 2242–2245, 1997.

[51] L. Tong, R. R. Gattass, J. B. Ashcom, S. He, J. Lou, M. Shen, I. Maxwell, and E. Mazur, "Subwavelength-diameter silica wires for low-loss optical wave guiding," *Nature*, vol. 426, no. 6968, pp. 816–819, 2003.

[52] F. Warken, E. Vetsch, D. Meschede, M. Sokolowski, and A. Rauschenbeutel, "Ultra-sensitive surface absorption spectroscopy using sub-wavelength diameter optical fibers," *Optics Express*, vol. 15, no. 19, pp. 11952–11958, 2007.

[53] R. E. R. Gonzáles, E. F. Chillcce, and L. C. Barbosa, "Micro-size tapered silica fibers for sensing applications," in *SPIE Photonic Devices+ Applications*, pp. 81200K–81200K, International Society for Optics and Photonics, 2011.

[54] D.-I. Yeom, E. C. Mägi, M. R. Lamont, M. A. Roelens, L. Fu, and B. J. Eggleton, "Low-threshold supercontinuum generation in highly nonlinear chalcogenide nanowires," *Optics letters*, vol. 33, no. 7, pp. 660–662, 2008.

[55] O. Aktaş, *Chalcogenide micro and nanostructures and applications*. PhD thesis, Bilkent University.

[56] A. Zakery and S. R. Elliott, *Optical nonlinearities in chalcogenide glasses and their applications*, vol. 135. Springer, 2007.

[57] C. R. Petersen, U. Møller, I. Kubat, B. Zhou, S. Dupont, J. Ramsay, T. Benson, S. Sujecki, N. Abdel-Moneim, Z. Tang, *et al.*, "Mid-infrared supercontinuum covering the 1.4–13.3 μm molecular fingerprint region using ultra-high na chalcogenide step-index fibre," *Nature Photonics*, vol. 8, no. 11, pp. 830–834, 2014.

[58] S. Shabahang, M. P. Marquez, G. Tao, M. U. Piracha, D. Nguyen, P. J. Delfyett, and A. F. Abouraddy, "Octave-spanning infrared supercontinuum

generation in robust chalcogenide nanotapers using picosecond pulses," *Optics letters*, vol. 37, no. 22, pp. 4639–4641, 2012.

[59] D.-I. Yeom, E. C. Mägi, M. R. Lamont, M. A. Roelens, L. Fu, and B. J. Eggleton, "Low-threshold supercontinuum generation in highly nonlinear chalcogenide nanowires," *Optics letters*, vol. 33, no. 7, pp. 660–662, 2008.

[60] D.-I. Yeom, E. C. Mägi, M. R. Lamont, M. A. Roelens, L. Fu, and B. J. Eggleton, "Low-threshold supercontinuum generation in highly nonlinear chalcogenide nanowires," *Optics letters*, vol. 33, no. 7, pp. 660–662, 2008.

[61] T. Schreiber, J. Limpert, H. Zellmer, A. Tünnermann, and K. Hansen, "High average power supercontinuum generation in photonic crystal fibers," *Optics Communications*, vol. 228, no. 1, pp. 71–78, 2003.

[62] H. Wei, H. Chen, S. Chen, P. Yan, T. Liu, L. Guo, Y. Lei, Z. Chen, J. Li, X. Zhang, *et al.*, "A compact seven-core photonic crystal fiber supercontinuum source with 42.3 w output power," *Laser Physics Letters*, vol. 10, no. 4, p. 045101, 2013.

[63] H. Chen, H. Wei, T. Liu, X. Zhou, P. Yan, Z. Chen, S. Chen, J. Li, J. Hou, and Q. Lu, "All-fiber-integrated high-power supercontinuum sources based on multi-core photonic crystal fibers," *IEEE Journal of Selected Topics in Quantum Electronics*, vol. 20, no. 5, pp. 64–71, 2014.

[64] B. Türedi, *All-chalcogenide core-shell fibers for nonlinear applications*. PhD thesis, Bilkent University.

[65] A. Ghatak and K. Thyagarajan, *An introduction to fiber optics*. Cambridge university press, 1998.

[66] D. Akbulut, *Lasing action and supercontinuum generation in nano-and micro-structures*. PhD thesis, Bilkent University.

[67] M. Yaman, T. Khudiyev, E. Ozgur, M. Kanik, O. Aktas, E. O. Ozgur,

H. Deniz, E. Korkut, and M. Bayindir, "Arrays of indefinitely long uniform nanowires and nanotubes," *Nature materials*, vol. 10, no. 7, pp. 494–501, 2011.

[68] M. Belal, L. Xu, P. Horak, L. Shen, X. Feng, M. Ettabib, D. Richardson, P. Petropoulos, and J. Price, "Mid-infrared supercontinuum generation in suspended core tellurite microstructured optical fibers," *Optics letters*, vol. 40, no. 10, pp. 2237–2240, 2015.

[69] J. Travers, "Blue extension of optical fibre supercontinuum generation," *Journal of Optics*, vol. 12, no. 11, p. 113001, 2010.

[70] B. J. Eggleton, B. Luther-Davies, and K. Richardson, "Chalcogenide photonics," *Nature photonics*, vol. 5, no. 3, pp. 141–148, 2011.

[71] J. S. Sanghera, L. B. Shaw, and I. D. Aggarwal, "Chalcogenide glass-fiber-based mid-ir sources and applications," *IEEE Journal of Selected Topics in Quantum Electronics*, vol. 15, no. 1, pp. 114–119, 2009.